Research article

Elucidating the anti-cancer potential of *Cinnamomum tamala* essential oil against non-small cell lung cancer: A multifaceted approach involving GC-MS profiling, network pharmacology, and molecular dynamics simulations

Debajani Mohanty [a], Sucheesmita Padhee [a], Arpita Priyadarshini [a],
Bibhuti Bhusan Champati [a], Prabhat Kumar Das [a], Sudipta Jena [a], Ambika Sahoo [a],
Pratap Chandra Panda [a], Sanghamitra Nayak [a], Asit Ray [a],*

[a] *Centre for Biotechnology, Siksha 'O' Anusandhan (Deemed to be University), Kalinga Nagar, Bhubaneswar, 751003, India*

ABSTRACT

Cinnamomum tamala (Buch.-Ham.) T.Nees & Eberm., or Indian Bay Leaf, is a well-known traditional ayurvedic medicine used to treat various ailments. However, the molecular mechanism of action of *Cinnamomum tamala* essential oil (CTEO) against non-small cell lung cancer (NSCLC) remains elusive. The present study aims to decipher the molecular targets and mechanism of CTEO in treating NSCLC. GC-MS analysis detected 49 constituents; 44 successfully passed the drug-likeness screening and were identified as active compounds. A total of 3961 CTEO targets and 4588 anti-NSCLC-related targets were acquired. JUN, P53, IL6, MAPK3, HIF1A, and CASP3 were determined as hub genes, while cinnamaldehyde, ethyl cinnamate and acetophenone were identified as core compounds. Enrichment analysis revealed that targets were mainly involved in apoptosis, TNF, IL17, pathways in cancer and MAPK signalling pathways. mRNA expression, pathological stage, survival analysis, immune infiltrate correlation and genetic alteration analysis of the core hub genes were carried out. Kaplan-Meier overall survival (OS) curve revealed that HIF1A and CASP3 are linked to worse overall survival in Lung Adenocarcinoma (LUAD) cancer patients compared to normal patients. Ethyl cinnamate and cinnamaldehyde showed high binding energy with the MAPK3 and formed stable interactions with MAPK3 during the molecular dynamic simulations for 100 ns. The MM/PBSA analysis revealed that van der Waals (VdW) contributions predominantly account for a significant portion of the compound interactions within the binding pocket of MAPK3. Density functional theory analysis showed cinnamaldehyde as the most reactive and least stable compound. CTEO exhibited selective cytotoxicity by inhibiting the proliferation of A549 cells while sparing normal HEK293 cells. CTEO triggered apoptosis by arresting the cell cycle, increasing ROS accumulation, causing mitochondrial depolarisation, and elevating caspase-3, caspase-8 and caspase-9 levels in A549 cells. The above study provides insights into the pharmacological mechanisms of action of *Cinnamomum tamala* essential oil against non-small cell lung cancer treatment, suggesting its potential as an adjuvant therapy.

---

* Corresponding author.
  E-mail address: asitray@soa.ac.in (A. Ray).

1. Introduction

Lung cancer causes the highest number of cancer-related fatalities globally, with non-small cell lung cancer (NSCLC) comprising more than 85% of all cases [1,2]. In 2020, there were 2.2 million new cases of lung cancer and 1.8 million reported deaths worldwide (GLOBOCAN, 2020). According to the Global Cancer Observatory study, India ranks fourth globally for lung cancer mortality (GLOBOCAN, 2020). Patients with NSCLC are mostly diagnosed at advanced stages due to constraints in early detection, which results in an overall survival rate of only 10–20% [3,4]. Managing lung cancer involves various treatment modalities, including chemotherapy, systemic therapy, radiotherapy, and surgery [5]. However, the possibility of recurrence and side effects associated with chemotherapy and radiation and emerging drug resistance underline the need for alternative effective treatment approaches [6,7]. Consequently, acquiring the underlying mechanisms behind NSCLC occurrence and progression is essential for developing novel anti-cancer drugs.

Natural product-based therapies have been proven effective for treating cancer. Several studies have shown that patients with non-small cell lung cancer receiving herbal supplements have increased survival rates [4,8]. Natural herbal scaffolds based hydrogels are being developed to control the initiation and progression of cancer [4,9].

The members of the genus *Cinnamomum* are economically tree species known for their commercial spice products. *Cinnamomum tamala* (Buch.-Ham.) Nees, commonly known as Indian Bay Leaf, is an evergreen tree of the family Lauraceae that grows wild in tropical and subtropical areas of Asia, Australia and the Pacific islands [10,11]. Essential oil is one of the active ingredients of the genus *Cinnamomum*. In Eastern and Western countries, dried leaves of *C. tamala* are used as a spice and flavouring agent in various food preparations. *C. tamala* bark has been used for thousands of years in traditional and Western medicine. *C. tamala* essential oil can be found in the stem, leaves, and bark. The essential oil has widespread applications in the cosmetic, pharmaceutical, and food industries. *Cinnamomum tamala* bark essential oil has been reported to possess antitumor, antiparasitic, antioxidant, anti-inflammatory and antiarthritic properties [12]. Several studies reveal that *C. tamala* exerts favourable anti-cancer effects. *In vitro* assay revealed *Cinnamomum tamala* bioactive constituents to exert cytotoxic effect against A549 (lung adenocarcinoma), MCF-7 (breast adenocarcinoma) and U-87MG (brain glioblastoma) cells [13]. *Cinnamomum tamala* leaf constituents exhibited antiproliferative activity against A2780 human ovarian cancer cells [14]. *Cinnamomum tamala* leaf extract showed anti-cancer activity against Ehrlich Ascites Carcinoma (EAC) bearing mice by reducing tumour growth [15]. A preclinical study has shown the anticancer potential of *Cinnamomum tamala* (Indian Bay Leaf oil) nanoemulsion and vitamin D-encapsulated cinnamon oil nanoemulsion on lung carcinoma cells (A549) [16]. Despite the claim on the anti-cancer activity of *C. tamala* (CTEO) essential oil, no significant study has been carried out to explain its mechanism against NSCLC. Like other herbal medicines, *Cinnamomum tamala* involves multiple components, targets, and pathways against cancer. However, the pharmacodynamic properties of the active components of CTEO and the key molecular targets responsible for its anti-cancer activity need to be fully explored.

Recently, understanding the molecular mechanism behind the onset and development of various diseases has improved with the application of network pharmacology. Network pharmacology has been employed to analyse phytoconstituent putative targets and disease-associated pathways [17]. The rationale for this research stems from the urgent need for innovative therapeutic approaches to enhance the effectiveness and safety of treating non-small cell lung cancer (NSCLC). *Cinnamomum tamala*, as a natural compound, represents a promising alternative that could address the limitations associated with conventional therapies. Through a combination of computational and experimental methodologies, this study aims to deepen our understanding of the molecular interactions between *Cinnamomum tamala* essential oil and NSCLC-related targets, as well as elucidate its potential mechanism of action. Furthermore, the utilisation of network pharmacology, molecular docking, and molecular dynamics simulations in the present study demonstrates the power of integrative approaches in drug discovery and development. Therefore, the current study aims to explore and identify bioactive constituents of *Cinnamomum tamala* essential oil that have the potential for treating non-small cell lung cancer. The interaction between the CTEO active constituents and the predicted targets was verified using molecular docking, density functional theory analysis and molecular dynamics approaches. In addition, *in vitro* experimental assays were performed to validate the anti-cancer effect of CTEO on A549 cancer cells.

2. Materials and methods

2.1. Sampling and essential oil extraction

The fresh barks of *C. tamala* were collected in July 2022 from Chauntra, Himachal Pradesh, India (32° 0′ 52.9992″ N, 76° 44′ 9.9996″ E, 1310 m a.s.l). The plant material was authenticated by Dr. P.C. Panda, and the specimen with voucher no (2453/CBT) was deposited in the Herbarium of the same institute. The extraction of essential oil from dried bark was carried out by hydrodistillation following the protocol mentioned in European Pharmacopoeia [18]. The collected essential oil was kept in dark vials at 4 °C for further analysis.

2.2. Chemical characterisation of the essential oil

The chemical analysis of *Cinnamomum tamala* bark essential oil was performed in a Clarus 580 GC (PerkinElmer, USA) integrated with an SQ-8 MS detector. 0.1 μl of neat essential oil was injected into the system in splitless mode. Compound separation was performed on an Elite-5 MS capillary column of 30 m length, 0.25 mm i.d. and 0.25 μm thickness using helium carrier gas at 1 ml/min a flow rate. Initially, the column oven was programmed at 60 °C, then increased to 220 °C at 3 °C/min, and finally held for 7 min. The

detector and ion source temperatures were set at 150 and 250 °C, respectively. The mass spectra of the constituents were recorded in the electron ionisation mode at 70 eV. The constituents were identified by matching their mass spectra with the compound library (NIST/EPA/NIH Mass spectral library, version 2.0) and comparing experimental retention indices with bibliographic literature [19].

2.3. Network pharmacology

2.3.1. Pharmacokinetic screening of phytoconstituents
The phytoconstituents identified through GC-MS analysis underwent drug-like property screening using the online SwissADME web server (http://www.swissadme.ch/). Screening parameters included Lipinski's rule [20] and a minimum Abbott oral bioavailability (OB) score greater than 0.5. Phytoconstituents meeting both criteria were selected as bioactive constituents of CTEO.

2.3.2. Acquisition of compound and disease-related targets
Compound-related putative targets were obtained from the Swiss Target Prediction (STP) (http://www.swisstargetprediction.ch/) and the Comparative Toxicogenomics database (https://ctdbase.org/). NSCLC-associated targets were collected from DisGenet (https://www.disgenet.org/), Malacards (https://www.malacards.org/), GeneCards (https://www.genecards.org/) and Therapeutic Target Database (https://db.idrblab.net/ttd/). Additionally, the Gene Expression Omnibus (GEO) (https://www.ncbi.nlm.nih.gov/geo/) database of NCBI was used to access the mRNA expression profiles of NSCLC patients and normal patient samples by selecting the GSE21933 dataset. This dataset contained 42 samples, including 21 NSCLC patients and 21 normal lung tissue samples and were analysed using the GEO2R program. The dataset was based on the GPL6254 Phalanx Human OneArray platform and processed using the iDEP.96 (http://bioinformatics.sdstate.edu/idep96/) online web tool. Upregulated and downregulated differentially expressed genes (DEGs) were obtained using 'limma trend package' with the criteria log fold change (log2FC) ≥ 1 and false discovery rate (FDR) value < 0.05. The differentially expressed genes heat map, venn diagram, and volcano plot were obtained using the R package. Then, Venny 2.1.0 (https://bioinfogp.cnb.csic.es/tools/venny/) online tool was used to acquire the overlapping targets among compound-related targets, disease-related targets and DEGs obtained from the GEO database. These genes are considered key therapeutic targets for treating NSCLC.

2.3.3. Protein-protein interaction (PPI) network
The key therapeutic targets identified by overlapping two gene datasets were deposited to the STRING database (https://string-db.org/) with the species limited to "*Homo sapiens*". The network containing direct and indirect protein linkages obtained with 'high confidence' (≥ 0.7) of the minimum required interaction score was then exported to Cytoscape 3.9.1 software. The Cytohubba plug-in of Cytoscape 3.9.1 was employed to perform topological parameter screening of closely interlinked genes from the network based on the degree algorithm. The obtained genes were considered hub genes.

2.3.4. Construction of compound-disease-target network
The interrelationship between the bioactive constituents of CTEO and their predicted targets in the treatment of NSCLC was visualised by constructing a compound-target-disease network in Cytoscape 3.9.1. The network nodes represent the candidate compounds, while the edges represent the compound-target interactions. By employing the Cytoscape cytoNCA tool, key active constituents of CTEO were screened from the network based on the degree value.

2.3.5. GO and KEGG pathway enrichment analysis
The role of critical therapeutic targets in the biological system and signalling pathways were analysed by performing Gene Ontology (GO) and Kyoto Encyclopaedia of Genes and Genomes (KEGG) enrichment analysis. The intersecting genes were imported into ShinyGO v 0.77 (http://bioinformatics.sdstate.edu/go/) to predict the three GO categories (molecular functions, biological processes, cellular components) and KEGG pathways of therapeutic genes involved. The enrichment analysis cut-off value was $p < 0.05$ and FDR<0.01. The overlapping targets were mapped into KEGG mapper (https://www.genome.jp/kegg/mapper/) to highlight the relevant pathway and analyse the distinctive molecular mechanism within that pathway.

2.3.6. External validation of the hub target genes
The Gene Expression Profiling Interactive Analysis (GEPIA) webserver (http://gepia.cancer-pku.cn/) was used to analyse the differential expression of hub target genes in LUAD tissues and normal lung tissues. The hub genes were imported into the GEPIA database to analyse their mRNA expression level and associated pathological stage in the Lung Adenocarcinoma (LUAD) patients and normal patients provided by the TCGA (Cancer Genome Atlas) and GTEx (Genotype Tissue Expression) dataset. The significance of hub genes on the overall survival of LUAD was assessed from the Kaplan–Meier survival plot.

The Human Protein Atlas (https://www.proteinatlas.org/) database was used to analzse the immune-histochemical investigation of hub genes. The protein expression of hub genes between NSCLC and normal lung tissues was compared based on staining intensity using specific antibodies. The relationship between the hub gene and immune infiltrates in the tumour microenvironment was investigated using TIMER 2.0 (http://timer.cistrome.org/).

2.4. In silico analysis

2.4.1. Molecular docking

The protein targets related to 'Human' were searched in the Uniprot database (https://www.uniprot.org/). The 3D structures of the proteins were downloaded from the RCSB PDB database (http://www.rcsb.org/pdb) in their PDB formats with low resolution and no mutation. The Prankweb server (https://prankweb.cz/) was used to analyse the active sites of the protein into which the ligand will bind. The native conformers of proteins were refined in Biovia Discovery Studio and Galaxyrefine web by eliminating water, ligands, ions, and heteroatoms and by filling missing residues. The energy minimization addition of polar hydrogen atoms and gasteiger charges to protein structures was performed using UCSF Chimera software. In the Autodock tool, the processed PDB files of proteins were converted into PDBQT format. The three-dimensional chemical structures of selected phytoconstituents were retrieved from the PubChem database in SDF formats and saved as PDB files in the Biovia discovery studio. The PDB files of the compounds were uploaded into the PyRx software using the in-built open Babel tool of the software. The energy minimization of the ligands was performed by applying a geometry optimisation force field. Then, the energy-reduced ligands were changed to ready-to-dock PDBQT formats. After preparing the PDBQT files of receptors and ligands for docking, a grid box was generated by setting X, Y, and Z coordinate values that were identified based on the measurement of pocket-1 from the PrankWeb server so that the ligand fix into the active site residues of proteins. Finally, each protein was subjected to docking with each ligand in the Autodock vina plugin tool of Pyrx software. The visualisation of docking results was done in Biovia Discovery Studio.

2.4.2. Molecular dynamics simulations

The MD simulation module created by SiBioLead LLP uses GROMACS simulation to assess the conformational deviation of docked protein-ligand complexes compared to uncomplexed apoprotein. The complexes were preprocessed by using the OPLS/AA force field [21]. The complex was embedded in a triclinic-type periodic boundary box containing a simple charge point (SPC) water solvation model and 0.15 M concentration of NaCl as counterions. The systems were energy minimized using the Steepest Descent algorithm for 5000 steps and equilibrated with NVT/NPT ensembles. All simulations were performed at 300 k temperature and 1 bar pressure. Finally, the complexes were simulated with the leapfrog algorithm for 100 ns, and the simulated trajectories were interpreted using an in-built GROMACS analysis package. Root mean square fluctuation (RMSF), root mean square deviation (RMSD), solvent accessible surface area (SASA), and radius of gyration (Rg) were measured to assess the stability of molecular docking simulations [22].

2.4.3. Density functional theory analysis

The chemical reactivity and stability of key active constituents of CTEO were predicted by applying density functional theory (DFT) analysis. The complete geometry optimisation of the chemical constituents was performed in Gaussian 09W software using B3LYP/*6-31G (d, p) basis set*. The theoretical quantum chemical parameters were calculated to assess the stability and reactivity of the constituents. The optimized chemical structures and level energy (HOMO, LUMO) of bioactive constituents were calculated using Avogadro software.

2.5. Anticancer assays

2.5.1. Cell culture

A549 (Human alveolar lung adenocarcinoma cell line) and HEK-293 (Human embryonic kidney cell line) were purchased from NCCS, Pune, India. Cells were cultured in Dulbecco Modified Eagle medium (DMEM) provided with 10 % Fetal bovine serum (FBS) and 1% penicillin and streptomycin at 37 °C in a humidified incubator containing 5% (v/v) CO_2.

2.5.2. Cell viability assay

The MTT (3-(4,5-Dimethylthiazol-2-yl)-2,5-diphenyltetrazolium bromide) assay was carried out to determine the cell cytotoxicity [23]. HEK-293 and A549 cells were allowed to grow in 96-well culture dishes for 24 h. The cultured cells were treated with CTEO (6.25, 12.5, 25, 50, 100 µg/ml) and incubated for 24 h in a humidified incubator. The used media was removed, and MTT reagent was added and incubated for another 3 h at 37 °C. Then, the formazan crystals were solubilized by adding 100 µl of DMSO. The absorbance was measured using an ELISA plate reader at 570 nm. The IC_{50} value of the above experiment was calculated using a linear regression equation.

2.5.3. Apoptosis assay

The extent of apoptosis was determined using FITC-labelled annexin V by flow cytometry as described previously with some modifications [24]. A549 cells (5×10^5 cells/2 ml) were inoculated into culture plates and maintained at 37 °C for 24 h, followed by exposure to CTEO (6 µg/ml) for 24 h. After treatment, cells were rinsed twice with PBS (phosphate buffer saline), followed by the addition of 100 µl of staining buffer (5 µl Annexin V-fluorescein isothiocyanate + 10 µl PI) and kept for 15 min at 37 °C. The cell apoptosis rate was analysed by flow cytometry (BD FACS Calibur, BD Biosciences, CA, USA).

2.5.4. Cell cycle analysis

Cell cycle phase distribution was done as described earlier [25]. A549 cells (5×10^5 cells/2 ml) were plated into culture dishes and treated for 48 h with CTEO at an IC_{50} concentration (6 µg/ml). After incubation, cells were harvested, rinsed twice with cold PBS and fixed with 1 ml of 70% ethanol at −20 °C for 30 min. The cells were then resuspended in PBS containing RNAase A (50 µg/ml) and

Propidium iodide (10 μg/ml) and incubated for 15–20 min. The samples were analysed using a flow cytometer (BD FACS Calibur, BD Biosciences, CA, USA).

2.5.5. Caspase expression assay

The caspase activity in A549 cells was determined as described earlier [26]. A549 cells (5×10^5 cells/2 ml) were allowed to grow in culture plates and maintained at 37 °C for 24 h. The cells were treated with IC_{50} concentration of CTEO (6 μg/ml) and incubated for 24 h. After incubation, the cells were harvested and rinsed twice with cold PBS, followed by the addition of 25 μl of 10 μM substrate solution (PhiPhiLux and CaspaLux kit; OncoImmunin, Inc., Gaithersburg, MD, USA). The cells were incubated at 37 °C for 60 min. Then, the cells were rinsed with 1X PBS and were studied using a flow cytometer (BD FACS Calibur, BD Biosciences, CA, USA).

Table 1
Chemical characterisation of *Cinnmamomum tamala* bark essential oil.

Compound	RT	RI$_{exp}$	RI$_{lit}$	Peak Area (%)
Benzaldehyde	6.42	957	960	0.6
Acetophenone	10.03	1066	1065	0.2
Terpinolene	11.11	1095	1088	0.8
Viridene	13.63	1156	1167	0.9
Borneol	14.13	1168	1169	0.2
cis-Linalool Oxide	14.40	1175	1174	0.2
α-Terpineol	15.05	1190	1188	0.3
Cinnamaldehyde	18.48	1270	1270	32.9
Z-Methyl cinnamate	18.81	1278	1299	1.4
n-Tridecane	19.76	1300	1300	0.2
δ-Elemene	20.93	1327	1338	0.2
Cyclosativene	22.35	1360	1371	0.2
α-Copaene	22.61	1367	1376	0.3
β-Elemene	23.20	1380	1390	0.4
Ethyl cinnamate	23.61	1390	1377	1.2
Longifolene	24.42	1409	1407	0.5
6,9-Guaiadiene	25.33	1431	1444	0.2
cis-Muurola-3,5-diene	25.63	1439	1450	0.3
α-Humulene	25.87	1445	1454	0.5
γ-Gurjunene	26.71	1465	1477	3.8
α-Amorphene	26.87	1469	1484	0.9
Amorpha-4,7(11)-diene	27.57	1486	1481	0.6
α-Muurolene	27.67	1489	1500	2.4
γ-Cadinene	28.22	1502	1513	2.7
δ-Cadinene	28.48	1509	1523	8.8
cis-Calamenene	28.57	1511	1529	1.3
γ-Amorphene	28.79	1517	1495	0.2
trans-Cadina-1,4-diene	28.98	1522	1534	0.6
α-Cadinene	29.14	1526	1538	1.5
α-Calacorene	29.31	1530	1545	2.0
β-Calacorene	30.11	1550	1565	0.1
Maaliol	30.66	1564	1567	0.6
Spathulenol	30.88	1570	1578	0.2
Guaiol	31.45	1585	1600	0.3
epi-Cedrol	31.80	1594	1619	0.2
Junenol	32.08	1601	1619	0.2
α-Corocalene	32.25	1605	1623	0.9
1-*epi*-Cubenol	32.66	1616	1628	1.2
Hinesol	33.21	1631	1641	1.1
Valerianol	33.28	1633	1658	1.0
cis-Calamenen-10-ol	33.38	1636	1661	0.7
α-Muurolol	33.72	1645	1646	2.8
2-Hydroxydiphenyl methane	34.30	1660	1675	0.1
Amorpha-4,9-dien-2-ol	36.01	1707	1700	0.1
Sesquiterpene hydrocarbons				29
Oxygenated Sesquiterpene				8.4
Monoterpene Hydrocarbon				0.2
Oxygenated Monoterpene				0.3
Phenylpropanoid				34.7
Furan				0.2
Benzenoid				1.8
Others				1
Total Identified				75.6

RT: Retention time in minutes.

RI$_{exp}$: Retention indices calculated on the basis of homologous n-alkane series (C_8–C_{20}) on an Elite-5 MS column.

RI$_{lit}$: Retention indices published in literature (Adams, 2007).

2.5.6. Measurement of intracellular reactive oxygen species (ROS)

The intracellular reactive oxygen species levels was evaluated using D2CFH-DA (2,7-dichlorofluorescein diacetate) dye as per the previously reported protocol [27] with slight modifications. Briefly, A549 cells were grown in a 60-mm culture dish and kept at 37 °C for 24 h. Then, the cells were exposed to IC_{50} concentration of CTEO (6 μg/ml) and again incubated for another 24 h. After treatment, the media was discarded and rinsed with PBS. The cells were resuspended in H2DCFDA ($2',7'$-dichlorofluorescein diacetate) solution for 30 min. Cells were harvested, centrifuged and washed with 1X PBS. ROS generation was measured to detect DCF intensity using a microscope (Carl Zeiss LSM 880, Germany).

2.5.7. Mitochondrial membrane potential assay

A549 cells were grown in culture plates and kept for 24 h in a CO_2 incubator. Then, the cells were exposed to IC_{50} concentration of CTEO (6 μg/ml) and incubated for another 24 h. After treatment, the used media was discarded and rinsed with PBS. The cells were incubated with JC-1 dye, counterstained with Hoechst 33342 solution and were visualised under the microscope (Carl Zeiss LSM 880, Germany).

Table 2
Pharmacokinetic screening of *Cinnamomum tamala* essential oil compounds.

Compound	Lipinski's rule				Violation	Drug likeness
	MW < 500 (g/mol)	MLOGP <4.15	HBA <10	HBD <5		
Benzaldehyde	106.12	1.45	1	0	0	Pass
Acetophenone	120.15	1.78	1	0	0	Pass
Terpinolene	136.23	3.27	0	0	0	Pass
Viridene	150.26	3.56	0	0	0	Pass
Borneol	154.25	2.45	1	1	0	Pass
cis-Linalool Oxide	170.25	1.38	2	1	0	Pass
α-Terpineol	154.25	2.3	1	1	0	Pass
Cinnamaldehyde	132.16	2.01	1	0	0	Pass
Z-Methyl cinnamate	162.19	2.2	2	0	0	Pass
n-Tridecane	184.36	5.67	0	0	1	Pass
δ-Elemene	204.35	4.53	0	0	1	Pass
Cyclosativene	204.35	5.8	0	0	1	Pass
α-Copaene	204.35	5.65	0	0	1	Pass
β- Elemene	204.35	4.53	0	0	1	Pass
Ethyl cinnamate	176.21	2.49	2	0	0	Pass
Longifolene	204.35	5.65	0	0	1	Pass
6,9-Guaiadiene	204.35	4.63	0	0	1	Pass
cis-Muurola-3,5-diene	204.35	4.63	0	0	1	Pass
α-Humulene	204.35	4.53	0	0	1	Pass
γ-Gurjunene	204.35	4.63	0	0	1	Pass
α-Amorphene	204.35	4.63	0	0	1	Pass
Amorpha-4,7(11)-diene	204.35	4.63	0	0	1	Pass
α-Muurolene	204.35	4.63	0	0	1	Pass
γ-Cadinene	204.35	4.63	0	0	1	Pass
δ-Cadinene	204.35	4.63	0	0	1	Pass
cis-Calamenene	202.34	5.45	0	0	1	Pass
γ-Amorphene	204.35	4.63	0	0	1	Pass
trans-Cadina-1,4-diene	204.35	4.63	0	0	1	Pass
α-Cadinene	204.35	4.63	0	0	1	Pass
α-Calacorene	200.32	5.36	0	0	1	Pass
β-Calacorene	200.32	5.36	0	0	1	Pass
Maaliol	222.37	3.81	1	1	0	Pass
Spathulenol	220.35	3.67	1	1	0	Pass
Guaiol	222.37	3.67	1	1	0	Pass
epi-Cedrol	222.37	3.81	1	1	0	Pass
Junenol	222.37	3.67	1	1	0	Pass
α-Corocalene	200.32	5.36	0	0	1	Pass
1-*epi*-Cubenol	222.37	3.67	1	1	0	Pass
Hinesol	222.37	3.67	1	1	0	Pass
Valerianol	222.37	3.67	1	1	0	Pass
cis-Calamenen-10-ol	218.33	3.46	1	1	0	Pass
α-Muurolol	222.37	3.67	1	1	0	Pass
2-Hydroxydiphenyl methane	184.23	3.34	1	1	0	Pass
Amorpha-4,9-dien-2-ol	220.35	3.56	1	1	0	Pass

MW: Molecular weight, HBA: Hydrogen bond acceptor, HBD: Hydrogen bond donor, MLOGP: Moriguchi otanol-water partition coefficien

2.6. AO/EtBr staining

Morphological observation by fluorescence microscopy was done as described earlier [24]. Briefly, A549 cells (2×10^5 cells/2 ml) were seeded onto Petri plates and maintained in a CO_2 incubator for 24 h. Then, the cells were exposed to IC_{50} concentration of CTEO (6 µg/ml) and incubated for another 24 h. Following treatment, the spent media was aspirated, and the cells were washed with PBS. Cells were harvested by trypsinisation and stained with 200 µl staining solution containing 1 ml of ethidium bromide and 20 µl of acridine orange in media for 10 min. The cell suspension was observed under a fluorescence microscope (Carl Zeiss, LSM 880, Germany).

2.7. Statistical analysis

The data are expressed as mean values and standard deviation (SD) based on three replicates (n = 3) using GraphPad Prism software.

3. Results and discussion

3.1. GC-MS analysis of Cinnamomum tamala bark essential oil

The *C. tamala* bark essential oil was pale yellowish with an oil yield of 0.35 (%v/w) on a dry weight basis. Forty-nine constituents
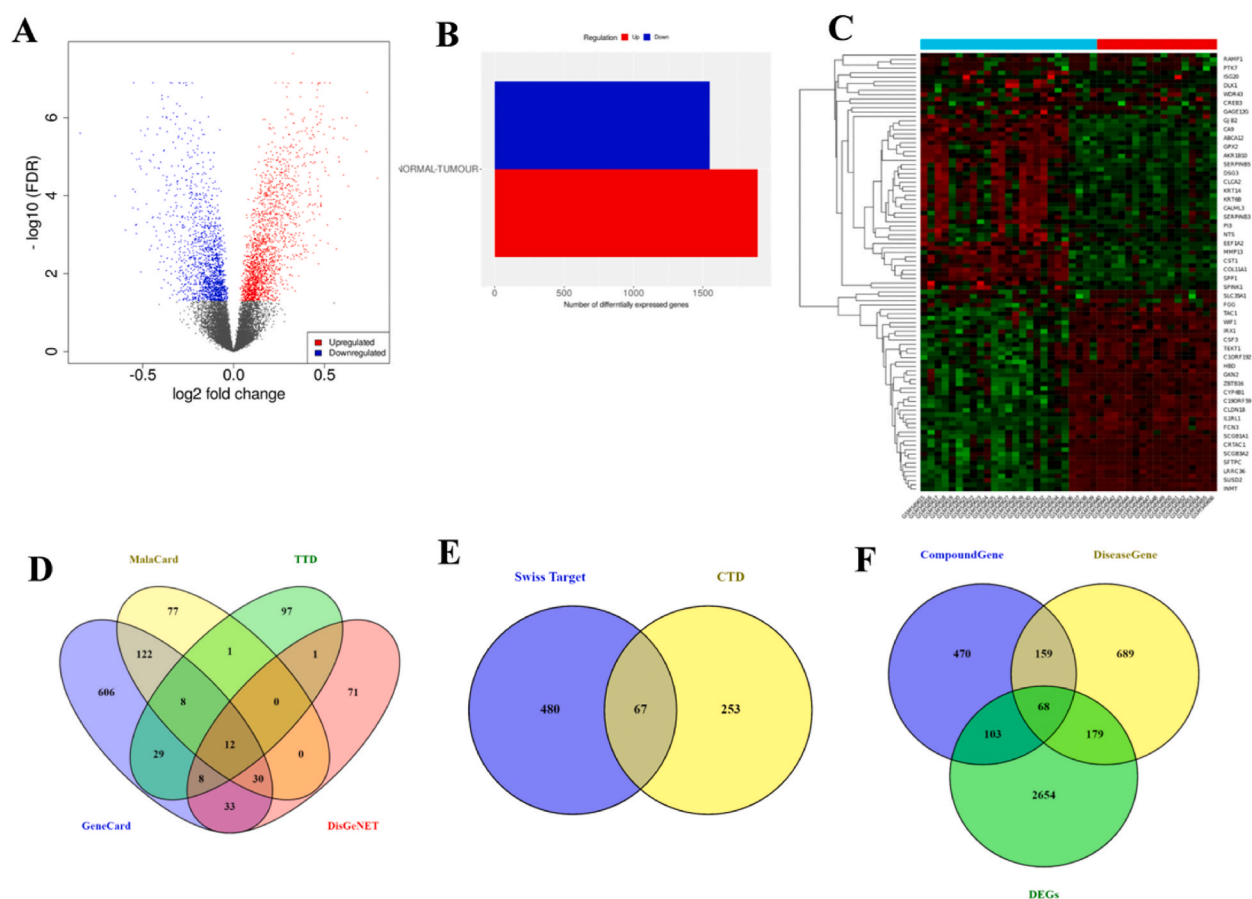
Fig. 1. Acquisition of compound and disease-related targets. (A) Volcano map of the distribution of all differentially upregulated (red) and downregulated genes (blue) in GSE21933 dataset. (B) Bar plot showing 1894 upregulated and 1548 downregulated genes in normal and tumour patients. (C) Heatmap of top 100 upregulated and downregulated genes. Upregulated genes are shown in red, and down regulated genes are shown in green color. (D) NSCLC-related targets obtained from Malacards, TTD, GeneCards and DisGenet databases. (E) Overlapping predictive targets of the CTEO active constituents obtained between Swiss Target Prediction (STP) and Comparative Toxicogenomics Database (CTD). (F) Venn diagram illustrating overlapping targets among CTEO (*Cinnamomum tamala* essential oil) targets, DEGs (Differentially Expressed Genes), and NSCLC (Non-Small Cell Lung Cancer) related targets, with a total of 68 genes. (For interpretation of the references to color in this figure legend, the reader is referred to the Web version of this article.)

were identified, accounting for 75.63% of the total essential oil. The major constituents were cinnamaldehyde (32.87%), δ-Cadinene (8.8%), γ-gurjunene (3.8%), α-muurolol (2.8%), γ-cadinene (2.7%) and α-muurolene (2.4%). All the identified constituents were broadly categorised into eight groups, including phenylpropanoids (34.70%), sesquiterpene hydrocarbons (29.0%), oxygenated sesquiterpenes (8.4%), benzenoids (1.8%), oxygenated monoterpenes (0.3%), monoterpene hydrocarbons (0.2%), furan (0.2%), and others (1%) (Table 1). *Cinnamomum cassia,* an important member of the genera *Cinnamomum,* also contains cinnamaldehyde as the principal constituent in its bark essential oil [28].

3.2. Network pharmacology

3.2.1. Drug-like screening of identified compounds and acquisition of compound and disease-related targets

Pharmacokinetic parameter screening is an important tool in drug discovery as it helps researchers to identify and develop safe and effective new drugs [29]. Out of 49 constituents identified by GC-MS, 44 constituents were filtered as biologically active as they qualified Lipinski's rule (molecular weight <500 amu, H-bond donor <10, H-bond acceptor <5, lipophilicity value < 5) and Abbott Oral Bioavailability score (≥0.5) (Table 2). Compounds that do not adhere to Lipinski Rule criteria are generally considered to have low druggability and are, therefore, unfavourable for oral consumption [30]. We tried to obtain differentially expressed genes (DEGs) in NSCLC by comparing the level of gene expressions between NSCLC and normal lung tissue samples. Based on the GSE21933 series of GEO dataset, 3438 differentially expressed genes were obtained, including 1894 upregulated and 1548 downregulated genes in NSCLC (Fig. 1A & B). The expression pattern of these DEGs is shown in a heat map (Fig. 1C). NSCLC-related targets were collected from disease-related online databases, namely GeneCards, Malacards, TTD and DisGeNET, which resulted in the identification of a total of 1417 targets (Fig. 1D). After removing duplications, a total of 4588 disease-related targets in NSCLC were obtained by combining targets from Genecards, Malacards, TTD, DisGenet and DEGs from the GEO database. The targets of bioactive constituents were predicted from two public databases i.e. Swiss target prediction (STP) and the Comparative toxicogenomics database (CTD). A total of
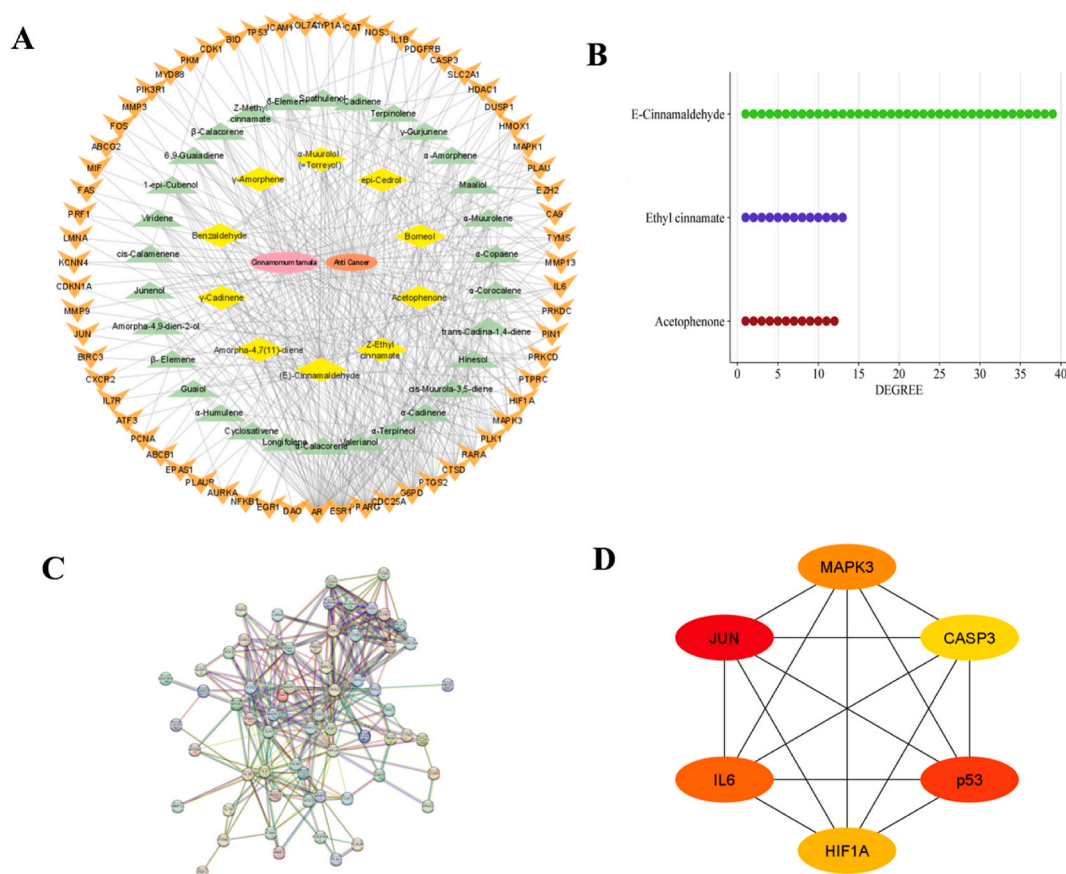

Fig. 2. Compound target network and protein-protein interaction (PPI) analysis. (A) Compound-target network analysis constructed using Cytoscape. Yellow diamonds represent the hub components of CTEO with high degree scores, green diamonds represent the components of CTEO with low degree scores, orange arrows represent the predictive targets of CTEO. (B) Dot bar plot demonstrating the top three hub compounds with the highest degree values. (C) The PPI network of 68 common overlapping targets was constructed using the STRING database (D) Topological screening of the PPI network showing 6 hub genes. (For interpretation of the references to color in this figure legend, the reader is referred to the Web version of this article.)

3961 predicted targets for CTEO were retrieved from STP and CTD. The common targets that existed between them were plotted using a Venn diagram (Fig. 1E). The intersection of compound targets of CTEO and disease-related targets of NSCLC included 68 targets that were considered key therapeutic targets for assessing the anti-cancer activity of CTEO (Fig. 1F).

3.2.2. Compound-target-disease network construction

The association between compounds of CTEO and their targets in the treatment of NSCLC was analysed and visualised by constructing a compound-target-disease network using Cytoscape 3.9.1. The constructed network includes 106 nodes and 425 edges (Fig. 2A). Then, the cytoNCA plug-in was used to filter out the key active constituents among the identified compounds based on the degree centrality algorithm. The selected top three hub compounds were cinnamaldehyde (Degree-39), ethyl cinnamate (Degree-13), acetophenone (Degree-12), with the highest degree values (Fig. 2B). Cinnamaldehyde and its natural derivatives have been shown to exert an anti-proliferative effect against tumour malignancies by modulating apoptotic pathways and arresting the cell cycle [31]. Cinnamaldehyde inhibits the proliferation of tumour cells and induces apoptosis by triggering the formation of reactive oxygen species [32,33]. Co-treatment of cinnamaldehyde and hyperthermia enhanced the production of ROS and MAPK phosphorylation in A549 cells [34]. Acetophenone has been shown to inhibit tumour cell growth and enhance the survivability of Swiss albino mice [35]. Overall, it was postulated that CTEO is a multicomponent herbal formulation with multi-target therapeutic effects.

3.2.3. Protein-protein interaction and topological analyses of hub genes

Sixty-eight overlapping targets were imported to the STRING database to obtain a PPI network to analyse the mechanism behind the therapeutic effect of CTEO against NSCLC. The network was achieved after removing the disconnected nodes at a high confidence level of 0.7. The resultant network was then analysed in Cytoscape 3.9.1, which contained 68 nodes and 240 edges (Fig. 2C). Then, Cytohubba plug-in was applied to perform the topological parameter screening of the PPI network. This analysis identified the top 6 genes ranked as hub genes, with the ranking based on the Maximal Clique Centrality (MCC) parameter. These genes were JUN, P53, IL6, MAPK3, HIF1A, CASP3 (Fig. 2D). JUN plays an essential role in tumour growth and progression by modulating several signalling pathways, including the MAPK signalling pathway [36]. p53 is a tumour suppressor gene, and its loss of function mutation leads to carcinogenesis [37]. Most human malignancies frequently exhibit mutations in the p53 gene, with p53 mutations accounting for over 50% of patients with non-small cell lung cancer (NSCLC) [38]. HIF-1A regulates cellular response to hypoxia and plays a critical role in regulating cell adhesion, angiogenesis and apoptosis [39]. HIF-1α overexpression leads to an increase in the invasion of human lung adenocarcinoma cells. MAPK3 protein belongs to the MAPK family and is associated with several cancer cells initiation, progression, and migration, including lung, thyroid, liver and gastric cancers [40]. IL6 has been found to promote metastasis in A549 cells and BALB/c lung metastasis mice model [41]. A study has shown that IL6 cytokine level was comparatively higher in NSCLC patients than in normal patients, and higher IL6 plasma level had a significantly poorer overall survival [42]. Caspase 3 is a cysteine-dependent protease of the caspase family that executes the major events of apoptosis and promotes tumorigenesis [43].

3.2.4. Pathway enrichment analysis

Gene ontology (GO) enrichment analyses of sixty-two overlapping targets were performed to explore various processes by which CTEO contributes to NSCLC treatment. A total of 1500 terms in GO: 1000 biological processes, 134 cellular components and 366
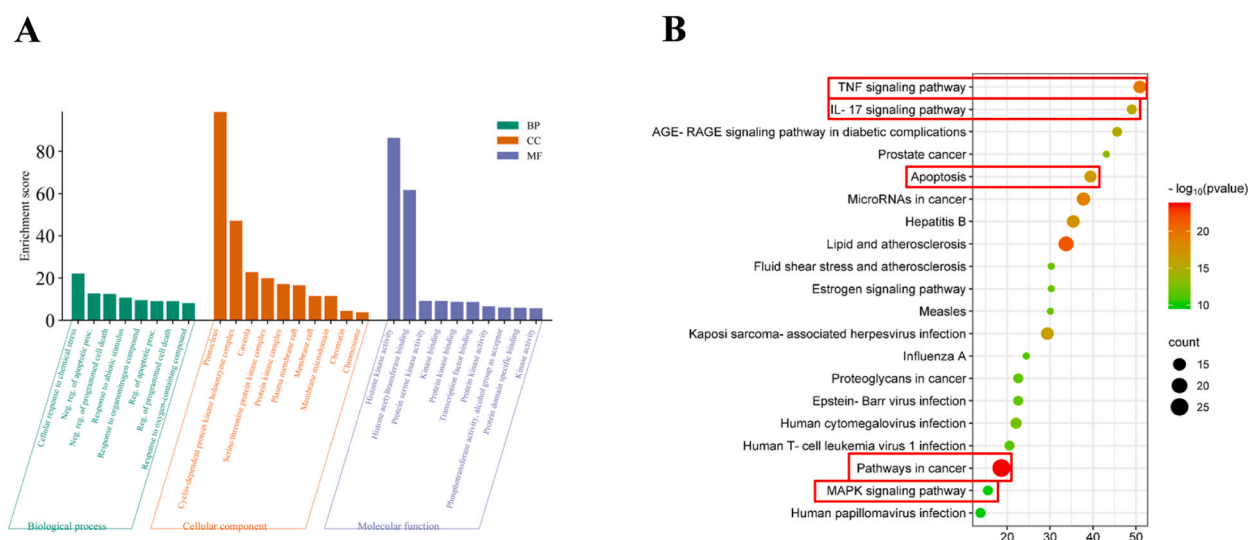

Fig. 3. Pathway enrichment analysis of common overlapping targets. (A) Gene ontology analysis demonstrating the top ten biological processes, molecular functions and cellular components, respectively. (B) KEGG pathway enrichment bubble plot displaying the top twenty biological pathways. Red rectangles correspond to relevant pathways related to NSCLC. (For interpretation of the references to color in this figure legend, the reader is referred to the Web version of this article.)

molecular functions were identified. The top ten enriched GO terms were obtained at a threshold of $p < 0.05$ and FDR<0.01 (Fig. 3A). Several highly enriched biological processes include regulation of cell death, apoptotic processes, programmed cell death, and response to endogenous stimulus. Similarly, highly enriched cellular components include chromosomes, chromatin, mitochondrion, membrane raft, membrane microdomain, anchoring junction, cell surface, etc. The key therapeutic targets associated with molecular functions encompass a range of functions, including kinase binding, double-stranded DNA binding, protein-containing complex binding, transcription factor binding, protein kinase binding, RNA polymerase II *cis*-regulatory region sequence-specific DNA binding and *cis*-regulatory region sequence-specific DNA binding.

In KEGG pathway enrichment analysis, 68 overlapping targets were found to be highly enriched for 105 signalling pathways at a threshold value of $p < 0.05$ and FDR<0.01. The top twenty enriched pathways were filtered based on their –logP values (Fig. 3B). The most relevant cancer-related pathways were the TNF signalling pathway, IL-17 signalling pathway, apoptosis, pathways in cancer and MAPK signalling pathway. MAPK pathway plays a decisive role in the carcinogenesis and treatment resistance of NSCLC cells by promoting proliferation or inhibiting apoptosis of these malignant cells [44–46]. The MAPK pathway assumes a greater significance in processes such as cell proliferation, differentiation, apoptosis, angiogenesis, and tumor metastasis when compared to other cellular pathways [47]. MAPK signalling pathway is a distinct signalling pathway that regulates cell proliferation, cell cycle advancement and survival [48]. *Boswellia sacra* essential oil has been shown to down-regulate the MAPK signalling pathway to exert its anti-cancer effect in human breast cancer cells [49]. Tumour necrosis factor (TNF) contributes to cancer by activating the NF-kB signalling pathway, which leads to the expression of anti-apoptotic and antioxidant genes. This activation results in suppressing c-Jun N-terminal kinase (JNK) activation, preventing cell death, and promoting cancer cell proliferation [50]. These data suggest that TNF might play a role in tumour growth, and could potentially serve as a marker for treatment response and prognosis in cancer patients. Apoptosis is a physiological process of programmed cell death, and inhibition apoptosis is a critical factor in the development of tumours [51]. Proper cell cycle regulation is essential for maintaining cell growth. Numerous studies have shown that dysregulation of the cell cycle is a common and critical event among various dysregulated pathways associated with lung carcinoma [52]. The cell cycle and apoptosis are interconnected processes, and cell cycle arrest can lead to apoptosis by modulating various regulatory proteins and signalling molecules. Previous reports have indicated that several essential oils possess anti-cancer properties by inducing cell cycle arrest and apoptosis [53–55].

3.2.5. External validation of hub target genes mRNA expression and evaluation of clinical relevance

The significant difference in the mRNA expression level of six hub genes between LUAD tissues and normal lung tissue was analysed using GEPIA database. The box plot analysis of six hub genes between LUAD tissues and normal lung tissue obtained from the GEPIA database showed that the mRNA expression level of p53 and CASP3 was significantly higher in tumour patients. In contrast the expression of JUN, IL6, MAPK3 and HIF1A was significantly lower in tumour tissues compared to the normal tissues (Fig. 4A). The result of stage plot analysis revealed that the level of HIF1A changed significantly with pathological stages and was higher especially ($p < 0.05$) in pathological stage III (Fig. 4B).

From the immune-histochemical analysis of hub genes, no difference was observed for IL6 and HIF1A expression between normal
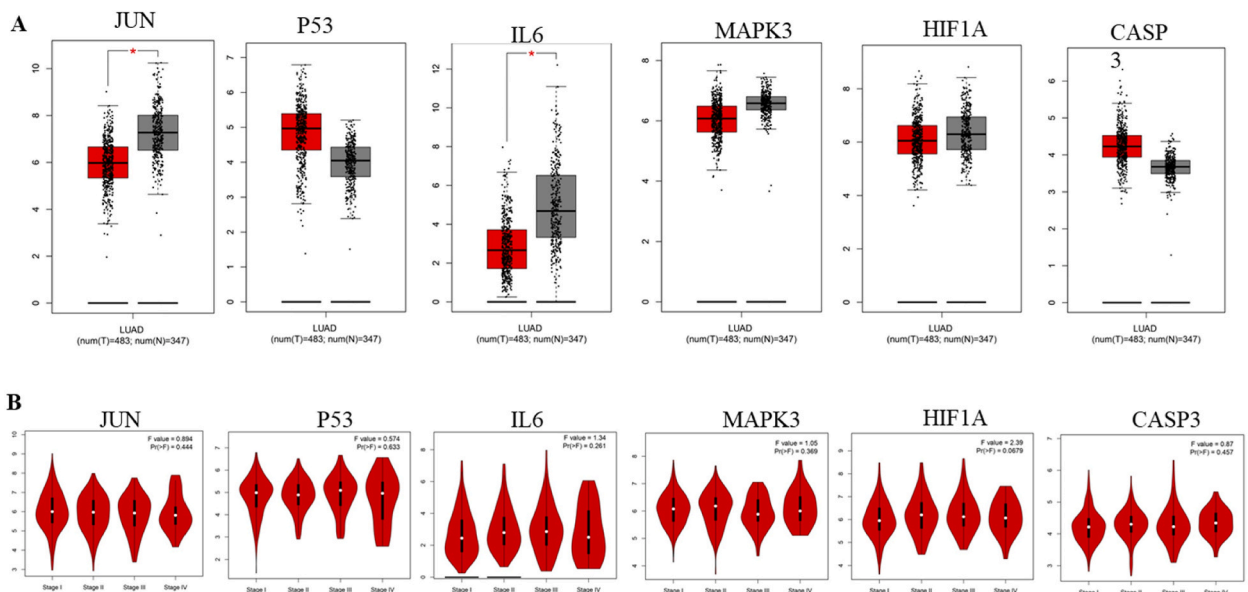

Fig. 4. mRNA expression profile and stage plot analysis of hub genes (A) Boxplot showing the mRNA expression levels of a) JUN b) P53 c) IL6 d) MAPK3 e) HIF1A f) CASP3 hub genes using GEPIA database between lung adenocarcinoma (red) and normal lung tissue (grey) samples. (B) The violin plots show the expression of hub genes a) JUN b) P53 c) IL6 d) MAPK3 e) HIF1A f) CASP3 in different pathological stages of lung cancer. (For interpretation of the references to color in this figure legend, the reader is referred to the Web version of this article.)
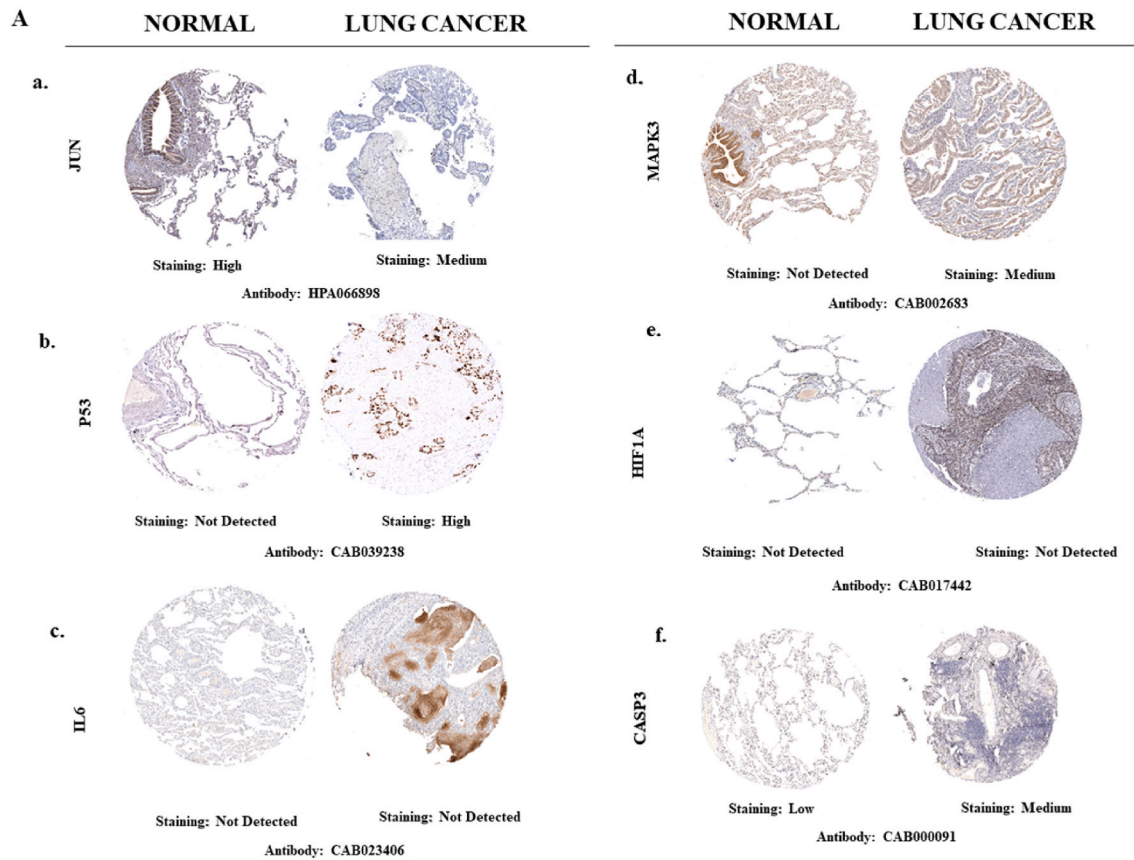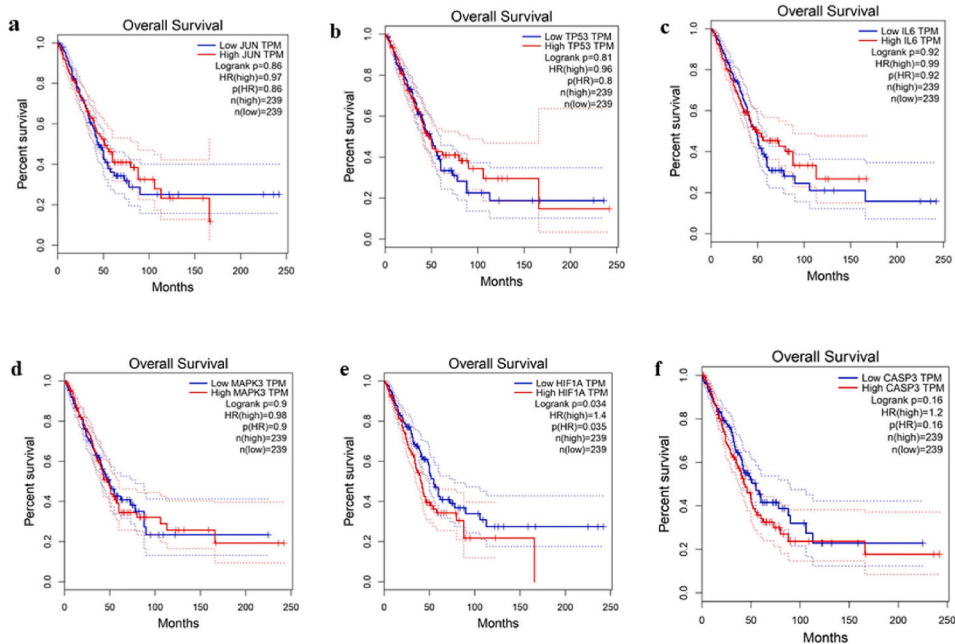
Fig. 5. Immunohistochemical and overall survival analysis of six hub genes. (A) Representative immunohistochemistry (IHC) images of (a) JUN (b) P53 (c) IL6 (d) MAPK3 (e) HIF1A (f) CASP3 genes in normal lung tissues and lung cancer tissues obtained from Human protein atlas database (HPA) include. (B) Kaplan-Meier overall survival plot for the six hub genes (a) JUN (b) P53 (c) IL6 (d) MAPK3 (e) HIF1A (f) CASP3.
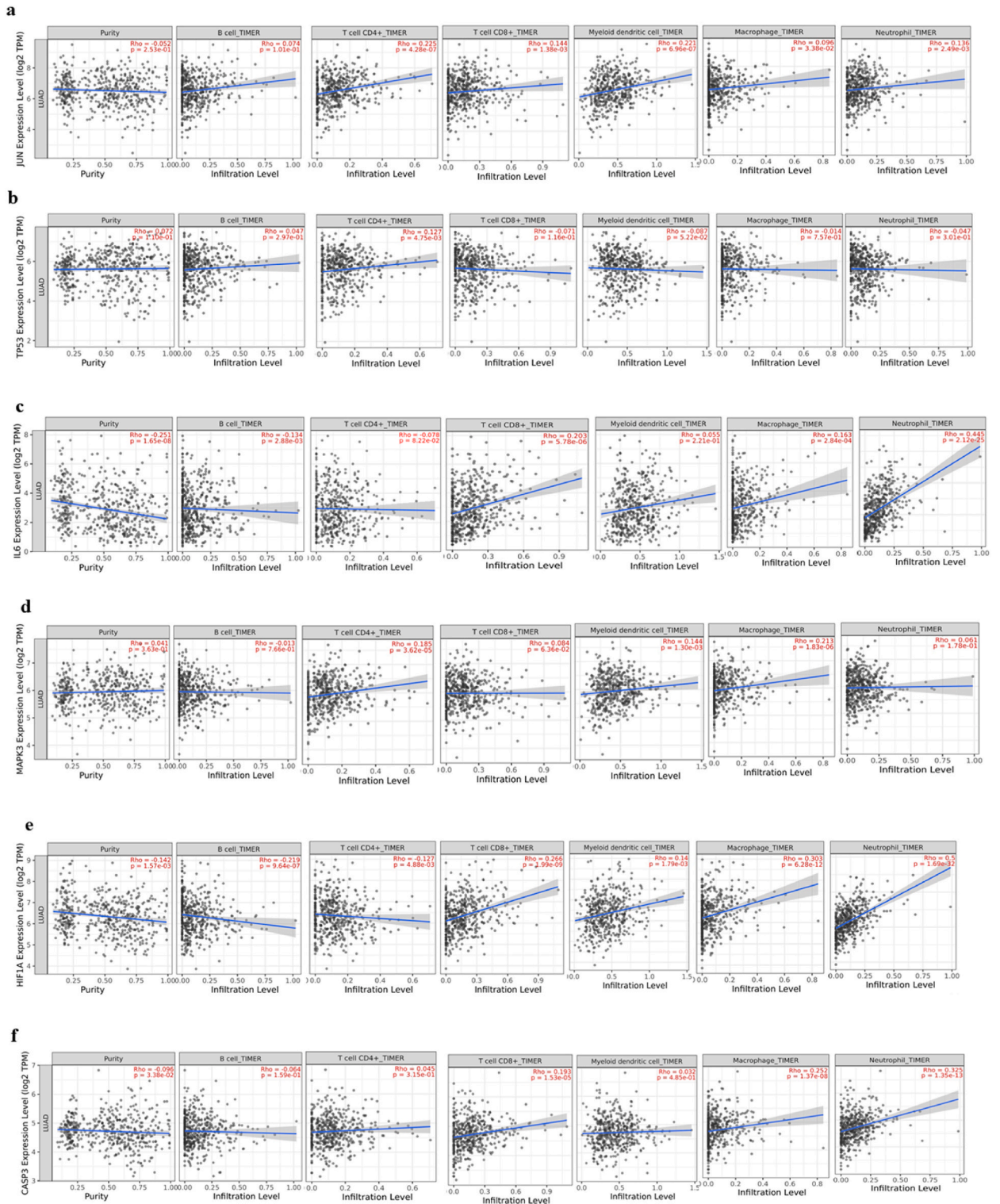
Fig. 6. Immune cell infiltrate analysis. The TIMER was used to evaluate the correlation between immune cell abundance and hub genes (a) JUN (b) p53 (c) IL6 (d) MAPK3 (e) HIF1A (f) CASP3 in lung cancer microenvironment.

tissue and LUAD tissue (Fig. 5A). The other four hub genes did not reveal significant differences in the expression level between normal tissue and NSCLC tissues. As compared to normal lung tissue, the expression of p53, MAPK3, and CASP3 increased in LUAD tissue, and the expression level of JUN decreased in LUAD tissue. The Kaplan-Meier survival curve analysis revealed that HIF1A (HR = 1.4, log-rank P = 0.034) and CASP3 (HR = 1.2, log-rank P = 0.16) were significantly overexpressed in LUAD tissues and, therefore, associated with poorer survival in patients diagnosed with LUAD (Fig. 5B).

The core mechanism of the immune microenvironment of NSCLC was analysed using TIMER 2.0 database. The correlation between the expression of hub targets and immune infiltrate has been demonstrated (Fig. 6A–F). Neutrophil was significantly correlated with the HIF1A (cor = 0.500, $p < 0.001$), IL6 (cor = 0.445, $p < 0.001$) and CASP3 (cor = 0.325, $p < 0.001$) expression levels. The above findings indicated that the hub targets are essential in regulating lung cancer.

The cBioPortal tool was used to investigate the gene alterations in the genomic profile of six hub genes in patients diagnosed with lung adenocarcinoma. It showed that 328 of 507 patients with lung adenocarcinoma had genetic variations in these hub targets (Fig. 7A). A summary of genetic alterations was also studied. The overall genetic alteration of 6 hub genes was 64.8%, and the individual genetic alteration rate varied from 2% to 52%. TP53 displayed the highest variation rate at 52%, while MAPK3 exhibited the lowest at 1.6%. Most gene alterations were mutations and multiple alterations; few were amplification and deep deletions (Fig. 7B).

3.3. Computational validation of selected compound-target interactions

3.3.1. Molecular docking

The information provided by network pharmacology was verified by performing molecular docking to identify the putative inhibitors to a particular protein. It analyses the binding affinities of the constituents with the target protein under consideration. On the basis of degree parameter screening of overlapping targets in the PPI network, key NSCLC-related gene targets (JUN, P53, IL6, MAPK3, HIF1A, and CASP3) and core compounds (cinnamaldehyde, ethyl Cinnamate, acetophenone) with top degree values in the compound-target network were selected for molecular docking studies. The PDB IDs considered for the proteins were JUN:5FV8, P53:1AIE, IL6:4CNI, MAPK3:4QTB, HIF1A:1H2M, CASP3:2XYG. A higher negative free binding energy corresponds to higher binding affinity between proteins and ligands [56]. The binding energies of all the confirmations ranged from −3.3 to −5.6 kcal/mol (Table 3). MAPK3 exhibited the highest binding affinity towards ethyl cinnamate with docking score of −5.6 kcal/mol. This interaction was attributed to hydrophobic interaction with ILE48 and LEU173 residues of MAPK3. Previously 17-β estradiol and deoxysappanone B 7,3′-dimethyl ether acetate formed hydrophobic interaction with LEU173 residue of MAPK3 [57]. Similarly, in the complex involving kaempferol 3-rutinoside-4′-glucoside and MAPK3, there was also evidence of hydrophobic interaction with the ILE48 residue of MAPK3 [58]. The binding free energy of MAPK3 with cinnamaldehyde was −5.5 kcal/mol. This interaction involved the formation of hydrogen bonds
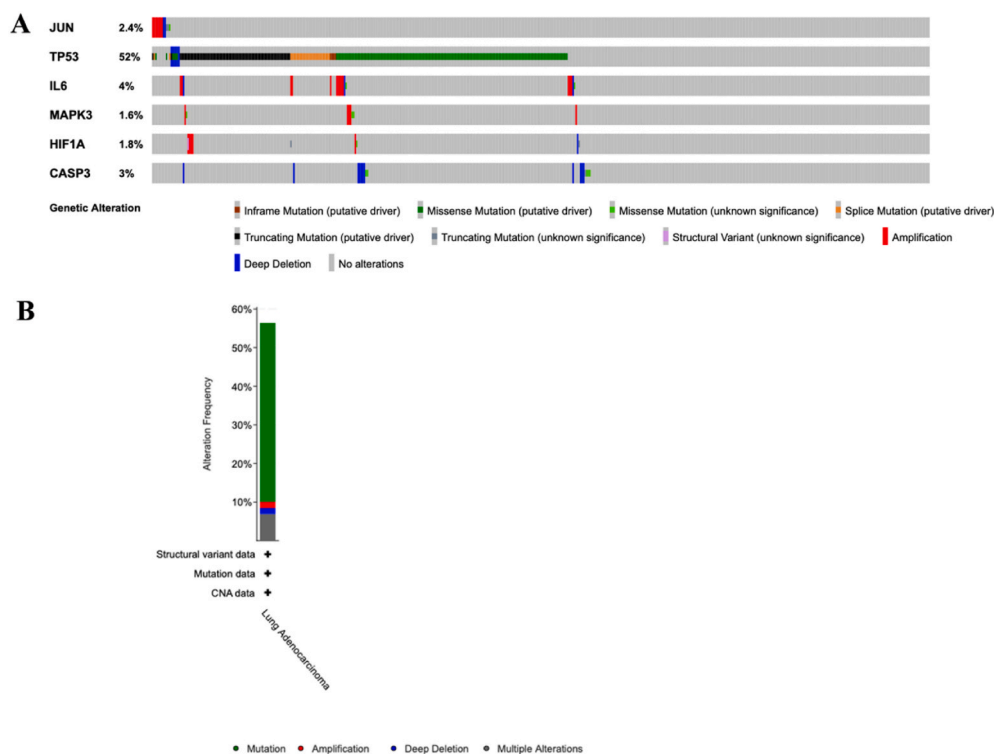

Fig. 7. Genetic alteration analysis of hub genes (A) Oncoprint summary generated using cBioportal representing the alteration in expression of six hub genes (B) Frequency of alteration in lung cancer genes.

Table 3

Binding affinities of proteins with ligands and co-crystalized ligands/inhibitors and their interacting residues.

Protein	Ligand/inhibitor	Binding affinity (Kcal/mol)	No. of H-bonds	H-bond interaction	Other interactions
JUN	Cinnamaldehyde	−5.2	2	LYS 22, GLU 25	PRO 37, ILE 24
	Ethyl cinnamate	−4.1	1	ARG 21	ILE 24
	Acetophenone	−4.9	1	PRO 37	ILE 24, ARG 21
	JNK–IN–7	−7.5	1	ASN 17	GLN 16, ARG 21, LEU 34
P53	Cinnamaldehyde	−4.1	1	GLU 346	ARG 342
	Ethyl cinnamate	−4.6	1	ASN 345	ARG 342
	Acetophenone	−4.2	1	LEU 330	PHE 338, ARG 342
	PAWI-2	−5.8	1	–	TYR 327
IL6	Cinnamaldehyde	−4.8	1	THR 85	GLU 105, PHE 83, LYS 103, LEU 104, GLN 166, ILE 106, ALA 84, PRO 40, GLU 165, LYS 39, GLN 38
	Ethyl cinnamate	−5.2	2	GLN 39, GLN 39	LYS 103, PRO 40
	Acetophenone	−4.8	–	–	THR 85, PRO 40, ALA 84, LYS 103, LEU 104, GLU 105, GLU 165, PHE 83, GLN 166, ILE 106
	TAM	−4.3	3	TYR 97, LYS 39, GLN 39	–
MAPK3	Cinnamaldehyde	−5.5	–	–	LEU 173, ALA 69, ILE 48, VAL 56
	Ethyl cinnamate	−5.6	–	–	LEU 173, ILE 48
	Acetophenone	−5.3	–	–	LEU 173, VAL 56, ALA 69
	PD98059	−7.9	–	LYS 71, SER 170	LEU 173, VAL 56, ILE 48, CYS 183, ASP 184
HIF1A	Cinnamaldehyde	−4	2	GLN 147, PHE 100	LEU 188
	Ethyl cinnamate	−3.4	–	–	TYR 102, LEU 188
	Acetophenone	−3.5	1	ASN 294	LEU 188
	OGA	−5.7	5	ASN 294, ASN 205, ASP 201, HIS 279, GLN 147	–
CASP3	Cinnamaldehyde	−3.6	1	GLU 123	ILE 160, ARG 164
	Ethyl cinnamate	−3.3	–	–	ILE 160, ARG 164, LEU 136, ILE 127, ALA 162
	Acetophenone	−3.6	1	GLY 125	ARG 164
	TQ8	−6	2	ARG 164, GLU 124	LEU136, PHE158, ILE160

with LYS71 and CYS183 and hydrophobic interactions with ALA69, ILE48, LEU173, and VAL56 residues of MAPK3. Hydrogen bonds in the protein-ligand complex indicate a higher level of interaction stability [59]. The interaction between MAPK3 and acetophenone was established by forming a hydrogen bond with MET125 and hydrophobic interactions with LEU173, VAL56 and ALA69 residues of MAPK3. The free binding energy of interaction was −5.3 kcal/mol. It is reported that vicenin-2, purvalonol and rutin also interacted
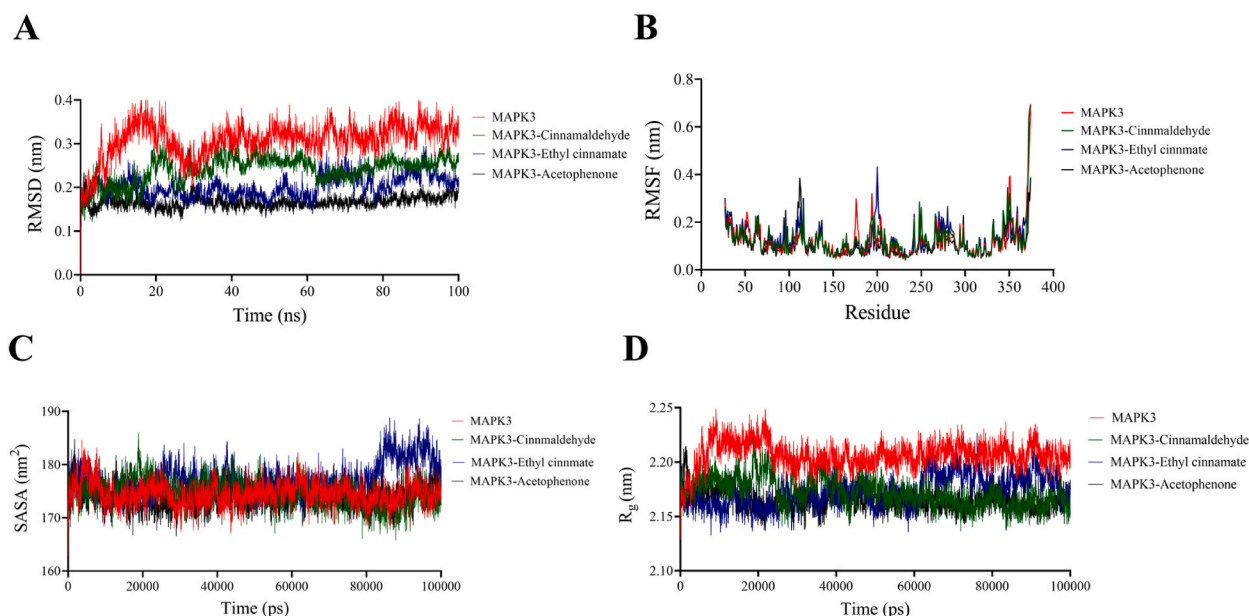

Fig. 8. Molecular dynamics simulation plots of apo-MAPK3 and selected three ligand-protein docked complexes over the period of 100 ns. Representative graphs include (A) Root mean square deviations (RMSD) of Cα atoms. (B) Root mean square fluctuation (RMSF) profile of Cα atoms. (C) Solvent accessible surface area (SASA). (D) Radius of gyration (R_g) over entire simulation period.

with VAL56, LEU173, ALA69, CYS183, ILE48 residues of MAPK3 by forming hydrophobic interactions [60]. Numerous hydrophobic residues surrounding the ligands within the binding pocket suggest that hydrophobic interactions play a role in stabilizing the complex.

3.3.2. Molecular dynamics (MD) simulation

The molecular docking result was validated by performing a molecular dynamics (MD) simulation of apoprotein (MAPK) with the top three selected drugs for 100 ns. Root mean square deviation (RMSD) of all alpha carbon atoms, root-mean-square-fluctuation (RMSF) of protein residue, solvent accessible surface area (SASA) and radius of gyration (Rg) of all protein-ligand complexes and apo-MAPK3 was investigated. Binding free energy calculation using MM/PBSA analysis of the docked complexes was also performed.

Root-mean-square deviation (RMSD) is a measure of the configurational stability of protein and ligands and also a measure of the extent of fluctuation in atomic position from the initial position. During the simulation, the RMSD fluctuation of the MAPK3-Cinamaldehyde complex increased to around 0.3 nm at 50 ns from the initial configurations and then remained stable around 0.25 nm from 50 to 60 ns with minor fluctuations till the end of the 100 ns simulation trajectory (Fig. 8A). In contrast, the MAPK3-acetophenone complex did not show sudden change or slippage throughout and was relatively stable throughout the simulation. Similarly, the MAPK3-ethyl cinnamate complex showed an average RMSD of 0.129 nm for the entire simulation\. Although small RMSD jumps appeared for the MAPK3-ethyl cinnamate complex as compared to the apo-MAPK3 protein, these changes did not affect the receptor binding ability, thus resulting in the complex stability.

Root-mean-square fluctuation (RMSF) analysis was carried out to analyse the impact of ligand binding on the flexible portion of the targeted protein residues. Unligated MAPK3, MAPK3-Cinnamaldehyde, MAPK3-ethyl cinnamate and MAPK3-acetophenone complexes experienced a similar type of fluctuation pattern during 100 ns MD simulation (Fig. 8B). Among these, a lower level of fluctuation was observed for the MAPK3-Acetophenone complex compared to all other complexes. In general, RMSF of amino acid residues of a target protein after binding with ligands should be around 0.2–0.3 nm without any notable fluctuations [61]. Most amino acid residues exhibit an RMSF value of less than 0.3 nm.

However, there are a few higher peaks in the middle and variations at the N and C terminal regions, which indicate the presence of loop regions. Conversely, regions with minimal fluctuations correspond to α-helices and β-strands, contributing to the overall rigidity of the protein structure.

Solvent accessible surface area (SASA) for the unbound protein and complexes was calculated to check the effect of the binding of the drug on the protein residue profile. The binding of a drug molecule to a protein may affect the structural properties, causing a change in SASA value. A greater SASA value indicates an expansion in protein structure and less protein stability. The average values of SASA corresponding to MAPK3-cinnamaldehyde (174.61 ± 2.43 nm^2) and MAPK3-ethyl cinnamate (177.15 ± 3.10 nm^2) complexes were slightly higher than the SASA value of unligated MAPK3 (174.55 ± 2.22 nm^2), thereby indicating slight expansion of MAPK3 during the course of interaction with cinnamaldehyde and ethyl cinnamate. However, the resulting SASA value of MAPK3-acetophenone complex (174.01 ± 2.25 nm^2) was observed to be slightly lower than that of apo-MAPK3 thereby suggesting that MAPK3 experienced less expansion in its structure upon interaction with acetophenone (Fig. 8C).

The radius of gyration (R_g) measures the protein's structural compactness and represents the root-mean-square distance between individual atoms from their axis of rotation. A lower extent of fluctuation during the simulation period suggests the protein structure's compactness and rigidity. A highly compact system encourages MD simulation system stability. The apo-MAPK3 experienced conformational fluctuation up to 20 ns from the initial state. MAPK3-Cinnamaldehyde complex followed a similar pattern like apo-MAPK3 after 60 ns (Fig. 8D). The MAPK3-ethyl cinnamate complex showed fluctuations in R_g value during 65–95 ns. MAPK3-acetophenone complex revealed structural compactness throughout the 100 ns simulation trajectory. Overall, Rg value confirms the stabilisation and suggests that ligand binding does not significantly alter the MAPK3 protein's overall structure, including the amino acid backbone and folding pattern arrangement.

The binding energy of the docked complexes and values of individual energy parameters are presented in Table 4. Individual energy parameters like van der Waals and electrostatic energy were measured using the MM/PBSA tool. The MAPK3-cinnamaldehyde complex has the highest average free binding energy of −18.48 kcal/mol. The average free binding energy was observed as −17.80 and −14.56 kcal/mol for MAPK3-Ethyl cinnamate and MAPK3-Acetophenone complex, respectively. The analysis of binding free energy showed that a significant portion of the ligand interactions in the MAPK3 binding pocket is attributed to van der Waals (VdW) contributions. Additionally, there were unfavourable polar contributions (EPB) for ligand binding, as indicated by the positive values obtained by MM/PBSA analysis.
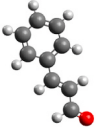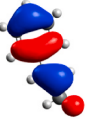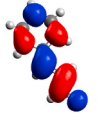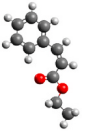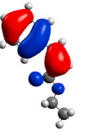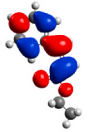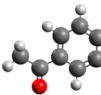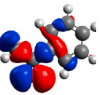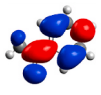
Table 4
MM-PBSA analysis of three selected docked complexes.

Complex	Vdwaals	EEL	EPB	ENPOLAR	ΔG Gas	ΔG Solv	ΔG Total
MAPK3-Cinnmaldehyde	−23.54	−1.41	8.36	−1.9	−24.94	6.46	−18.48
MAPK3-Ethyl cinnamate	−25.67	0.30	9.82	−2.24	−25.38	7.58	−17.80
MAPK3-Acetophenone	−20.81	−1.26	9.31	−1.79	−22.07	7.52	−14.56

ΔG is represented in Kcal/mol.

Vdwaals: Van der Waals interactions, EEL: Electrostatic Energy, EPB: Electrostatic Polarization Binding, ENPOLAR: Non-Polar Solvation Energy, ΔG Gas: Gas Phase Gibbs Free Energy, ΔG Solv: Solvation Gibbs Free Energy, ΔG Total: Total Gibbs Free Energy Change.

Table 5
Quantum chemical parameters for the top three compounds having the highest degree values.

Compound	Optimized structure	HOMO	LUMO	E HOMO (eV)	E LUMO (eV)	Δε (eV)	IE (eV)	EA (eV)	χ (eV)	μ (eV)	η (eV)	σ (eV)	ω (eV)
Cinnamaldehyde				−6.577	−2.088	4.489	6.577	2.088	4.333	−4.333	2.245	0.446	4.181
Ethyl cinnamate				−6.294	−1.698	4.596	6.294	1.698	3.996	−3.996	2.298	0.435	3.470
Acetophenone				−6.723	−1.474	5.249	6.723	1.474	4.099	−4.099	2.623	0.381	3.200

HOMO: Highest occupied molecular orbital, LUMO: Lowest unoccupied molecular orbital, E HOMO: energy of HOMO, E LUMO: energy of LUMO, Δε: energy gap between HOMO and LUMO, IE: ionisation energy, EA: electron affinity, χ: electronegativity, μ: chemical potential, η: chemical hardness, σ: chemical softness, ω: electrophilicity.

3.3.3. Conceptual DFT analysis

The stability and reactivity of core constituents of CTEO determined by network pharmacology were analysed in terms of frontiers molecular orbital analysis i.e. HOMO (highest occupied molecular orbital) and LUMO (Lowest unoccupied molecular orbital) as the energies of HOMO and LUMO are directly linked to the binding potential of the compounds. The HOMO denotes electron donors, while LUMO denotes electron acceptors [62]. Additionally, frontier molecular orbitals provide insight into molecular transition, chemical reactivity and their interaction with biological targets [63].

The extent to which an electron is excited from its ground state to an excited state is primarily determined by the energy gap between them, which plays a crucial role in electronic absorption processes [4]. The binding ability of a compound will increase if it has more HOMO and less LUMO energies. The energy gap is a factor derived from the HOMO and LUMO energy levels and has been found beneficial in determining the molecular stability and chemical reactivity of the molecule. The higher the energy gap value, the higher the molecular stability and the lower the reactivity. In this study, the calculated value of the energy gap is in order of aceto-phenone > ethyl cinnamate > cinnamaldehyde. Acetophenone exhibited the highest energy gap, whereas cinnamaldehyde showed the lowest energy gap value (Table 5). This suggests that cinnamaldehyde is the most reactive and least stable compound, while
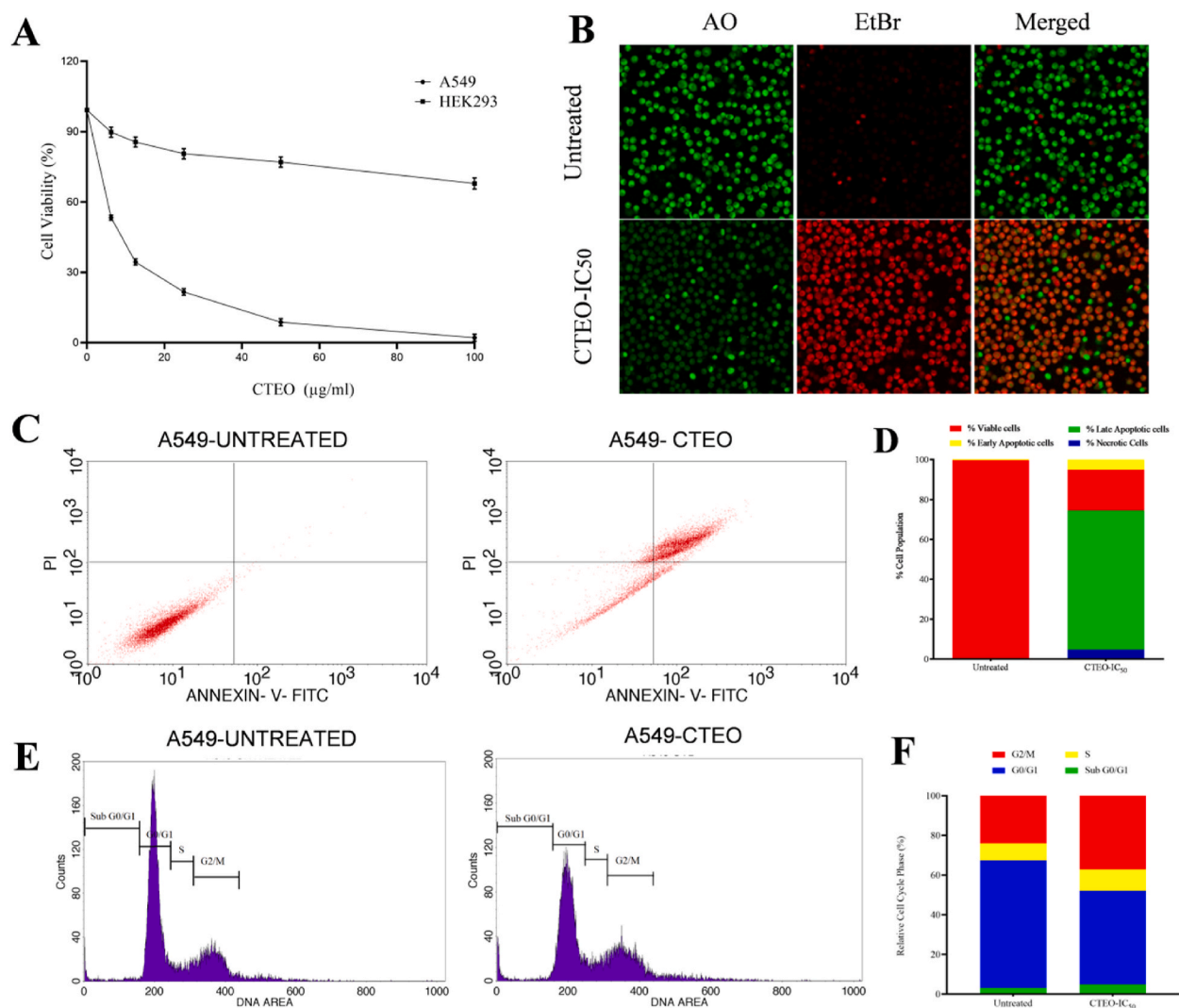

Fig. 9. Effect of CTEO on cell proliferation, apoptosis and cell cycle arrest of A549 cells (A) Cytotoxic effect of CTEO on HEK293 and A549 cells as measured by MTT assay. (B) Apoptosis-related morphological changes were assessed using AO/EtBr dual staining assay. Viable cells appear green and exhibit a normal cellular appearance. Early apoptotic cells appear green and display nuclear margination and chromatin condensation. Late apoptotic cells exhibit an orange colour and demonstrate fragmented chromatin and the presence of apoptotic bodies. (C) Apoptosis rate in un-treated and CTEO treated A549 cells as measured by annexin V-FITC/PI double labelling assay (D) Quantitative measurement of the percentage of viable, early apoptotic, late apoptotic, and necrotic cells in untreated and CTEO treated A549 cells. (E) Cell cycle distribution in untreated and CTEO-treated A549 cells. (F) Quantitative measurement of the percentage of cells distributed in different cell cycle phases. (For interpretation of the references to color in this figure legend, the reader is referred to the Web version of this article.)

acetophenone is the least reactive and most stable phytoconstituent.

The chemical hardness parameter can be predicted based on the energy gap value of a compound and hence associated with the stability and reactivity of the compound. The greater a molecule's $\Delta E_{LUMO-HOMO}$ value, the greater its chemical hardness. A molecule with low softness or high hardness is more reactive and less stable. The constituents exhibited chemical hardness in the order of cinnamaldehyde < ethyl cinnamate < acetophenone. Therefore, acetophenone is the hardest, and cinnamaldehyde is the softest compound.

The electronegativity of a compound is a crucial molecular descriptor as it influences the molecule's capacity to accept electrons. The greater the electronegativity, the greater its affinity to attract electrons. Therefore, a chemically reactive molecule has high electronegativity and less chemical potential. Chemical potential refers to a molecule's energy change in reference to the number of electrons in a fixed potential [64]. It explains the ability of a chemical constituent to exchange electrons with the surroundings in its ground state, and it is also linked to the compound's electrophilic index. The chemical potential of the essential oil constituents was in the order of cinnamaldehyde < acetophenone < ethyl cinnamate. Electrophilicity defines a molecule's potential for energy stabilisation when it gains additional electrons from its surroundings [65]. As a result, strong electrophiles have high electrophilicity values, while weak electrophiles have low electrophilicity values. A high electrophilicity index molecule, such as cinnamaldehyde, can be considered a good electrophile.

The properties of the phytochemicals, as determined through conceptual DFT calculations, correlate well with the docking analysis results. Cinnamaldehyde, the phytochemical with a high docking score, emerged as the constituent with a low energy gap, chemical hardness, and chemical potential when DFT-based molecular descriptors were also considered.

3.4. Experimental validation of the anti-cancer mechanism of CTEO in A549 cells

The cytotoxic effect of CTEO was assessed against normal cells (HEK293 cells) and non-small cell lung cancer cells (A549 cells) using MTT colorimetric assay. CTEO inhibited A549 cell proliferation in a concentration-dependent manner after the treatment period of 24 h. The observed IC_{50} value was 6.14 µg/ml for the A549 cell, as observed from the cell viability curve (Fig. 9A). The inhibitory activities of CTEO against HEK293 normal human cell was also analysed, which displayed a low cytotoxic effect of the essential oil, with IC_{50} value of 179.24 µg/ml. Therefore it can be inferred that CTEO was cytotoxic to A549 cells and non-toxic towards normal
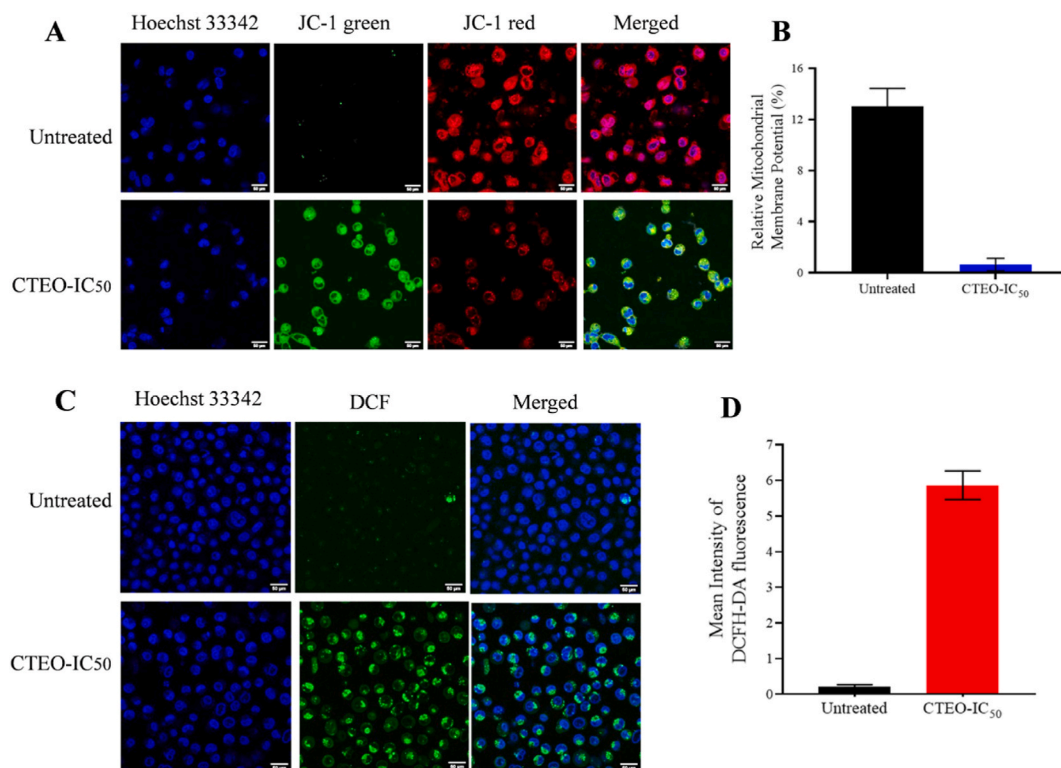

Fig. 10. Effect of CTEO treatment on mitochondrial membrane potential and ROS generation in A549 cells (A) Representing JC-1 staining images in untreated and CTEO-treated A549 cells observed under fluorescence microscope (B) Quantitative analysis of relative mitochondrial membrane in CTEO treated A549 cells compared to the untreated group. (C) Representative confocal images of DCF fluorescence intensity in untreated and CTEO-treated A549 cells. Bar represents 50 µm. (D) Quantitative analysis represented as mean DCFH-DA fluorescence intensity in untreated and CTEO-treated A549 cells.

HEK293 cells. Previous reports on *Cinnamomum* species have displayed good anti-tumor effects. For example, the commercial essential oil of *C. zeylanicum* exhibited an anti-proliferative effect on A549 cells with an IC_{50} value of 0.017% (v/v) [66]. *Cinnamomum cassia* essential oil significantly inhibited cell proliferation against the alveolar lung adenocarcinoma cell line (A549) with an IC_{50} value of 50.21 μg/ml [67].

Apoptosis, also known as programmed cell death, is required for multi-cellular organisms to maintain development and homeostasis by eliminating unwanted or extra cells. Deregulation of apoptosis contributes to the pathogenesis of tumours by allowing neoplastic cells to survive despite hypoxia and oxidative stress. To investigate the effects of CTEO on cell apoptosis, the morphology of A549 cells treated with the CTEO was determined by staining with AO/EtBr. The nuclei of untreated cells showed consistent green fluorescence without CTEO, indicating healthy cells with intact nuclei. However, after 24 h treatment with CTEO, apoptotic cell count
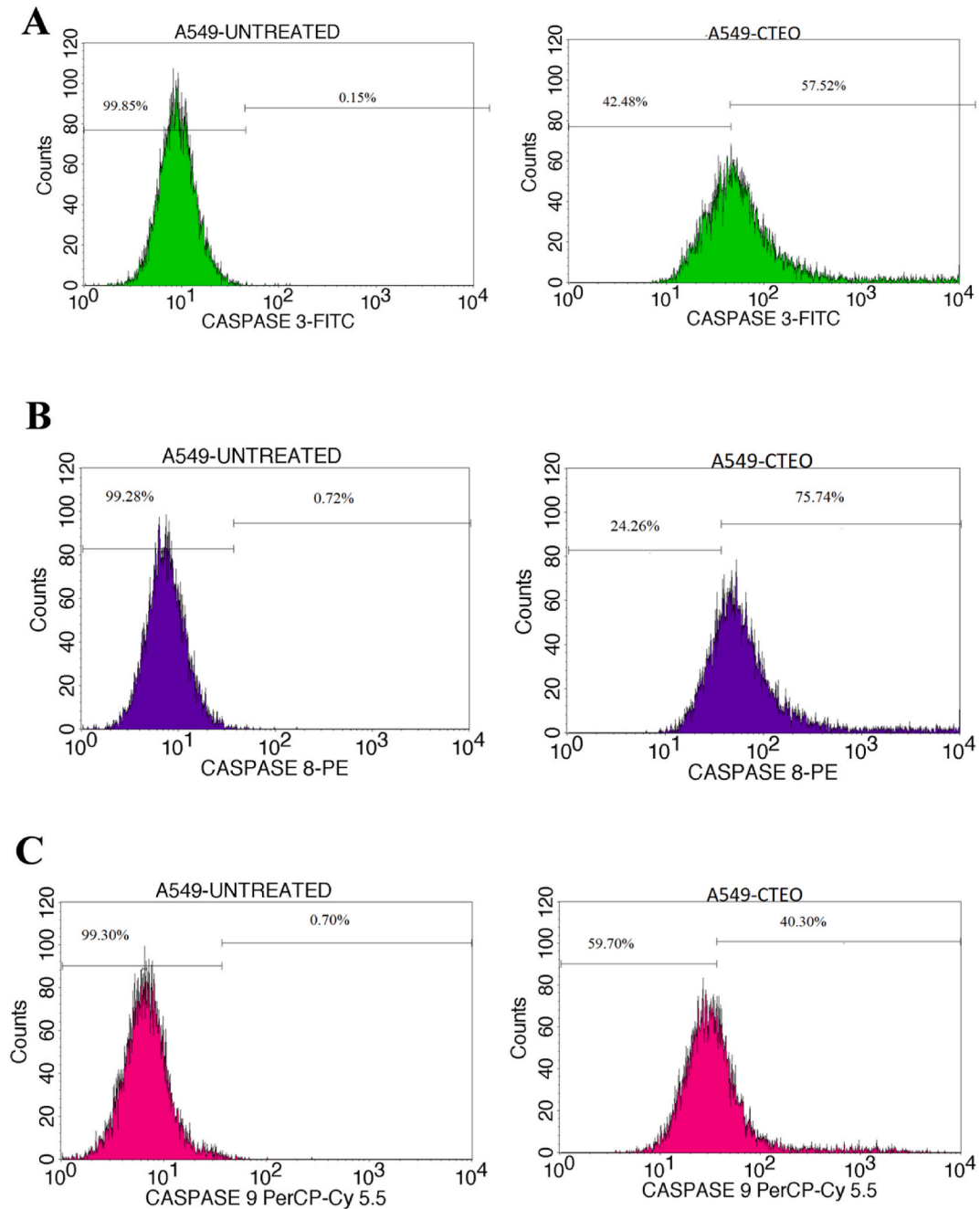

Fig. 11. Representative flow cytometry analysis of activated (A) caspase-3 (B) caspase-8, and (C) caspase-9 levels in untreated and CTEO-treated A549 cells.

increased significantly, as demonstrated by fragmentation and condensation of the nucleus. These findings revealed that cell death was caused by apoptosis. Viable cells with undamaged DNA and nucleus fluoresced green and non-viable cells with fragmented DNA and nucleus fluoresced red. The results of AO/EtBr staining assays are shown in Fig. 9B. Additionally, the percentage of apoptotic cells was determined using Annexin-V FITC/PI dual staining assay. The assay detects the loss of asymmetry in the phospholipid membrane, thereby indicating the possibility of apoptosis [68]. Annexin-V binds specifically to phosphatidylserine (PS) residues and is usually used with propidium iodide (PI) to discriminate between early and late apoptotic cells [69]. After 24 h of incubation with CTEO (6 μg/ml), a significant increase in the proportion of late and early apoptotic A549 cells was observed (Fig. 9C). The late and early apoptotic cell percentage increased significantly to 69.67% and 5.06% after treatment with CTEO (6 μg/ml) compared to the untreated group (Fig. 9D). These data suggested that CTEO can cause apoptosis in A549 cells.

Cancer is typically associated with abnormalities in cell cycle regulation. A fundamental change in genetic regulation of cell division results in unrestricted cell proliferation and ultimately leads to cancer development [70]. The effect of CTEO on the cell cycle distribution of A549 cells in different phases was investigated by flow cytometry analysis following 24 h of incubation (Fig. 9E). As depicted in Fig. 9F, when A549 cells are treated with CTEO (6 μg/ml), the proportion of arrested cells in Sub G0/G1, S and G2/M phases increased from 3.17%, 8.57% and 23.97% in the untreated group to 4.93%, 10.73% and 37.19% in CTEO treated cells, respectively. Furthermore, CTEO treatment reduced the percentage of cells in G0/G1 phase from 64.29% in the untreated group to 47.15% in CTEO-treated cells. This observation suggests that CTEO induced cell apoptosis may be due to cell cycle arrest at the G2/M phase. Previously, *Cinnamomum cassia* dried twigs have been reported to induce G2/M phase cell cycle arrest in A549 cells [70].

Mitochondria are involved in various cellular processes and functions, critical in determining cell survival or death [71]. The cells were stained with mitochondria membrane potential-specific JC-1 dye to investigate the changes in mitochondrial membrane potential resulting from apoptosis. As illustrated in Fig. 10A, viable cells with high mitochondrial membrane potential elicit red fluorescence due to JC-1 accumulation, and apoptotic cells elicit green fluorescence as JC-1 exists in monomeric form due to decreased membrane potential. Treatment of A549 cells with CTEO (6 μg/ml) showed a decreased mitochondrial membrane potential compared to the untreated group, indicating a loss or depolarisation of mitochondrial membrane potential. Quantitative analysis of membrane potential revealed that CTEO treatment decreased the aggregate/monomer ratio from 13.02 ± 1.14 in the untreated group to 0.64 ± 0.49 in the CTEO-treated group (Fig. 10B). Depolarisation of mitochondrial membrane is one of the primary events of cell apoptosis [72]. The above result indicates that CTEO caused a loss in mitochondrial membrane potential. The intrinsic pathway of apoptosis is initiated by the loss of mitochondrial membrane potential, which, in turn, leads to the release of cytochrome *c* and subsequently activates downstream caspases that finally lead to the establishment of apoptosis. Deregulation in mitochondrial activation of caspases results in disturbed apoptotic cell death, which is seen in several types of cancer cells [73].

Reactive oxygen species radicals can cause direct damage to cells or act as an intermediate signalling molecule by inducing oxidative stress [74]. Reactive oxygen species (ROS) perform dual functions at the cellular level, i.e., by maintaining redox homeostasis and activating various downstream signalling pathways [75]. Excessive ROS causes dysfunction and depolarisation of the mitochondrial membrane, which leads to mitochondria-driven cell apoptosis [76]. The change in intracellular ROS levels was assessed using a 2′,7′-dichlorodihydrofluorescein diacetate (H2DCFDA) assay to determine whether the mitochondrial membrane depolarisation was associated with ROS generation. The fluorescence microscopic observation revealed that treatment of A549 cells with CTEO (6 μg/ml) increased the percentage of cells expressing DCF intensity to $5.86 \pm 0.40\%$ compared to the untreated group (Fig. 10C and D). This result indicates that ROS production could cause CTEO-mediated cell death.

The sequential activation of caspases plays a key process in executing apoptosis. Caspases act as critical mediators of apoptosis, and their inactivation can contribute to tumorigenesis [77]. Among different caspases, caspase 3 is a prototypical executioner caspase, when activated by the initiator caspases, cleaves other functional cell-associated proteins, leading to apoptotic cell death. The involvement of caspases in CTEO-induced cell apoptosis was assessed by measuring the level of active caspase-3, caspase-8 and caspase-9 in A549 cells treated with CTEO (6 μg/ml) using flow cytometry. Flow cytometry analysis revealed that CTEO treatment significantly increased the percentage of cells expressing caspase-3, caspase-8 and caspase-9 from $0.15 \pm 0.09\%$, $0.72 \pm 0.47\%$ and $0.70 \pm 0.29\%$ in the untreated group to $57.52 \pm 2.92\%$, $75.74 \pm 2.29\%$ and $40.30 \pm 1.85\%$ in CTEO treated cells, respectively (Fig. 11A–C). The above result indicated a significant increase in caspase 8, caspase 3 and caspase 9. expression levels. All these findings suggest that CTEO triggers apoptosis in A549 cells through mitochondrion-mediated intrinsic and extrinsic pathways.

4. Conclusion

In summary, an integrative approach of metabolomics, network pharmacology, bioinformatics and experimental assays was carried out to decipher the multi-component, multi-target, multi-pathway pharmacological mechanism of CTEO in treating NSCLC. Cinnamaldehyde, ethyl cinnamate and acetophenone may be the key bioactive constituents behind the anti-cancer activity of CTEO. The pharmacological mechanism of CTEO treating NSCLC was strongly associated with 6 hub genes (JUN, P53, IL6, MAPK3, HIF1A, and CASP3), which were linked to TNF, IL17, apoptosis, pathways in cancer and MAPK3 signalling pathways. The experimental studies revealed that CTEO effectively inhibits cell proliferation, causing apoptotic cell death and cell cycle arrest of A549 cells. However, we have limited information on how these bioactive constituents contribute to the anti-proliferative and apoptotic activity of CTEO. Specifically, it is important to explore whether components such as cinnamaldehyde from CTEO actively participate in pathway regulation. Additionally, research should aim to identify core targets and pathways beyond the apoptotic pathway, including those related to TNF and IL17 pathway to gain a comprehensive understanding of CTEO's anti-cancer mechanisms. Furthermore, conducting research using animal models will be crucial to validate the anti-cancer potential of CTEO. Overall, the above result suggested that CTEO might be utilised in treating NSCLC and will serve as a preliminary basis for the rational use of CTEO for further clinical trials.

Funding

This work received no funds or any extramural research grants.

Ethical approval

This study does not involve the need for ethical approval. The research ethics committee has confirmed that no ethical approval is required.

Consent to participate

Not applicable.

Consent for publication

Not applicable.

Data availability statement

Data will be made available on request.

CRediT authorship contribution statement

Debajani Mohanty: Writing – original draft, Conceptualization. **Sucheesmita Padhee:** Methodology, Formal analysis. **Arpita Priyadarshini:** Writing – original draft. **Bibhuti Bhusan Champati:** Methodology, Formal analysis. **Prabhat Kumar Das:** Methodology, Formal analysis. **Sudipta Jena:** Writing – review & editing. **Ambika Sahoo:** Writing – review & editing. **Pratap Chandra Panda:** Writing – review & editing. **Sanghamitra Nayak:** Writing – review & editing. **Asit Ray:** Supervision.

Declaration of competing interest

The authors declare that they have no known competing financial interests or personal relationships that could have appeared to influence the work reported in this paper.

References

[1] R.S. Herbst, D. Morgensztern, C. Boshoff, The biology and management of non-small cell lung cancer, Nature 553 (2010) 446–454, https://doi.org/10.1038/nature25183.

[2] M.H. Widyananda, S.K. Pratama, R.S. Samoedra, F.N. Sari, V.D. Kharisma, A.N.M. Ansori, Y. Antonius, Molecular docking study of sea urchin (*Arbacia lixula*) peptides as multi-target inhibitor for non-small cell lung cancer (NSCLC) associated proteins, J Pharm Pharmacogn Res 9 (4) (2021) 484–496.

[3] Y. Wang, Y. Zhang, Y. Wang, X. Shu, C. Lu, C. Shao, X. Liu, C. Yang, J. Luo, Q. Du, Using network pharmacology and molecular docking to explore the mechanism of Shan Ci Gu (*Cremastra appendiculata*) against non-small cell lung cancer, Front. Chem. 9 (2021) 1–14, https://doi.org/10.3389/fchem.2021.682862.

[4] S. Kumar, F. Abbas, I. Ali, M.K. Gupta, S. Kumar, M. Garg, D. Kumar, Integrated network pharmacology and *in-silico* approaches to decipher the pharmacological mechanism of *Selaginella tamariscina* in the treatment of non-small cell lung cancer, Phytomed. plus. 3 (2) (2023), https://doi.org/10.1016/j.phyplu.2023.100419.

[5] Y. Zhang, Y. Yao, Y. Fu, Z. Yuan, X. Wu, T. Wang, Z. Hong, Y. Yang, H. Wu, Inhibition effect of oxyepiberberine isolated from *Coptis chinensis* franch. on non-small cell lung cancer based on a network pharmacology approach and experimental validation, J. Ethnopharmacol. 278 (2021) 1–11, https://doi.org/10.1016/j.jep.2021.114267.

[6] S. Sadeghi, A. Davoodvandi, M.H. Pourhanifeh, N. Sharifi, R. ArefNezhad, R. Sahebnasagh, S.A. Moghadam, A. Sahebkar, H. Mirzaei, Anti-cancer effects of cinnamon: insights into its apoptosis effects, Eur. J. Med. Chem. 178 (2019) 131–140, https://doi.org/10.1016/j.ejmech.2019.05.067.

[7] R.F. Xie, Z.Y. Song, L.Y. Xu-Shao, J.G. Huang, T. Zhao, Z. Yang, The mechanism of Bai He Gu Jin Tang against non-small cell lung cancer revealed by network pharmacology and molecular docking, Medicine 101 (52) (2022) 1–9.

[8] J.W. Ho, Y. Leung, C. Chan, Herbal medicine in the treatment of cancer, Curr. Med. Chem. 2 (2) (2002) 209–214, https://doi.org/10.2174/1568011023354164.

[9] G. Feger, B. Angelov, A. Angelova, Prediction of amphiphilic cell-penetrating peptide building blocks from protein-derived amino acid sequences for engineering of drug delivery nanoassemblies, J. Phys. Chem. B 124 (20) (2020) 4069–4078, https://doi.org/10.1021/acs.jpcb.0c01618.

[10] S.R. Mir, M. Ali, R. Kapoor, Chemical composition of essential oil of *Cinnamomum tamala* Nees et Eberm. leaves, Flavour Fragrance J. 19 (2004) 112–114, https://doi.org/10.1002/ffj.1236.

[11] J. Wang, B.S. Su, H. Jiang, N. Cui, Z. Yu, Y. Yang, Y. Sun, Traditional uses, phytochemistry and pharmacological activities of the genus *Cinnamomum* (Lauraceae): a review, Fitoterapia 146 (2020) 1–46, https://doi.org/10.1016/j.fitote.2020.104675.

[12] R.K. Upadhyay, Therapeutic and pharmaceutical potential of *Cinnamomum tamala. research reviews: Pharmacy and pharmaceutical Sciences* 6 (3) (2017) 18–28.

[13] D. Thanekar, J. Dhodi, N. Gawali, A. Raju, P. Deshpande, M. Degani, A. Juvekar, Evaluation of antitumor and anti-angiogenic activity of bioactive compounds from *Cinnamomum tamala: In vitro, in vivo* and *in silico* approach, South Afr. J. Bot. 104 (2016) 6–14, https://doi.org/10.1016/j.sajb.2015.09.014.

[14] D. Shahwar, S. Ullah, M.A. Khan, N. Ahmad, A. Saeed, S. Ullah, Anticancer activity of *Cinnamon tamala* leaf constituents towards human ovarian cancer cells, Pak. J. Pharm. Sci. 28 (3) (2015) 969–972.

[15] M.S. Saluja, B. Sangameswaran, A. Sharma, C. Dubey, Phytochemical study and *in-vitro* cytotoxic activity of *Cinnamomum tammala* Linn. Against Ehrlich Ascites carcinoma (EAC) and Dalton's Ascitic Lymphoma (DAL) cell lines, Res. J. Pharmacogn. Phytochem. 2 (1) (2010) 37–40.

[16] N. Meghani, P. Patel, K. Kansara, S. Ranjan, N. Dasgupta, C. Ramalingam, A. Kumar, Formulation of vitamin D encapsulated cinnamon oil nanoemulsion: its potential anti-cancerous activity in human alveolar carcinoma cells, Colloids Surf. B Biointerfaces 166 (2018) 349–357, https://doi.org/10.1016/j.colsurfb.2018.03.041.

[17] A.A. El-Banna, R.S. Darwish, D.A. Ghareeb, A.M. Yassin, S.A. Abdulmalek, H.M. Dawood, Metabolic profiling of *Lantana camara* L. using UPLC-MS/MS and revealing its inflammation-related targets using network pharmacology-based and molecular docking analyses, Sci. Rep. 12 (2022) 1–17, https://doi.org/10.1038/s41598-022-19137-0.

[18] European Pharmacopoeia, seventh ed., Council of Europe, Strasbourg, 2011, pp. 1160–1161.

[19] R.P. Adams, Identification of Essential Oil Components by Gas Chromatography/Mass Spectroscopy, Allured Publishing Corporation: Carol Stream, IL, USA, 2007.

[20] C.A. Lipinski, Lead-and drug-like compounds: the rule-of-five revolution, Drug Discov. Today Technol. 1 (4) (2004) 337–341, https://doi.org/10.1016/j.ddtec.2004.11.007.

[21] S.M. Nayeem, E.M. Sohail, G. Ridhima, M.S. Reddy, Target SARS-CoV-2: computation of binding energies with drugs of dexamethasone/umifenovir by molecular dynamics using OPLS-AA force field, Res. Biomed. Eng. 38 (2021) 1–10, https://doi.org/10.1007/s42600-020-00119-y.

[22] D.C. Rapaport, The Art of Molecular Dynamics Simulation, Cambridge university press, 2004.

[23] S. Jena, A. Ray, O. Mohanta, P.K. Das, A. Sahoo, S. Nayak, P.C. Panda, *Neocinnamomum caudatum* essential oil ameliorates lipopolysaccharide-induced inflammation and oxidative stress in RAW 264.7 cells by inhibiting NF-κB activation and ROS production, Molecules 27 (23) (2022) 1–20, https://doi.org/10.3390/molecules27238193.

[24] A. Ray, A. Gadnayak, S. Jena, A. Sahoo, J. Patnaik, P.C. Panda, S. Nayak, Hedychium spicatum rhizome essential oil induces apoptosis in human prostate adenocarcinoma PC-3 cells via mitochondrial stress and caspase activation, Heliyon 9 (3) (2023) e13807, https://doi.org/10.1016/j.heliyon.2023.e13807, 1, 18.

[25] A. Ray, S. Jena, B. Dash, A. Sahoo, B. Kar, J. Patnaik, P.C. Panda, S. Nayak, N. Mahapatra, *Hedychium coronarium* extract arrests cell cycle progression, induces apoptosis, and impairs migration and invasion in HeLa cervical cancer cells, Cancer Manag. Res. 11 (2019) (2019) 483–500.

[26] Y.C. Ko, J.C. Lien, H.C. Liu, S.C. Hsu, B.C. Ji, M.D. Yang, W.H. Hsu, J.G. Chung, Demethoxycurcumin induces the apoptosis of human lung cancer NCI-H460 cells through the mitochondrial-dependent pathway, Oncol. Rep. 33 (5) (2015) 2429–2437, https://doi.org/10.3892/or.2015.3865.

[27] D. Mohanty, S. Padhee, C. Sahoo, S. Jena, A. Sahoo, P.C. Panda, S. Nayak, A. Ray, Integrating network pharmacology and experimental verification to decipher the multitarget pharmacological mechanism of Cinnamomum zeylanicum essential oil in treating inflammation, Heliyon 10 (2) (2024) e24120, https://doi.org/10.1016/j.heliyon.2024.e24120, 1, 25.

[28] X. Deng, Q. Liao, X. Xu, M. Yao, Y. Zhou, M. Lin, P. Zhang, Z. Xie, Analysis of essential oils from cassia bark and cassia twig samples by GC-MS combined with multivariate data analysis, Food Anal. Methods 7 (2014) 1840–1847, https://doi.org/10.1007/s12161-014-9821-y.

[29] A. Anju Kumar, P. Yadav, U. Navik, V. Jaitak, Chemical composition, *in vitro* and *in silico* evaluation of essential oil from *Eucalyptus tereticornis* leaves for lung cancer, Nat. Prod. Res. 37 (10) (2023) 1656–1661, https://doi.org/10.1080/14786419.2022.2107642.

[30] M.H. Widyananda, C.A. Kurniasari, F.M. Alam, W.C. Rizky, T.G.A. Dings, A.N.M. Ansori, Y.a. Antonius, Exploration of potentially bioactive compounds from Fingerroot (*Boesenbergia rotunda* L.) as inhibitor of atherosclerosis-related proteins (CETP, ACAT1, OSC, sPLA2): an *in silico* study, Jordan J. Pharm. Sci. 16 (3) (2023) 550–564, https://doi.org/10.35516/jjps.v16i3.1609.

[31] S. Banerjee, S. Banerjee, Anticancer potential and molecular mechanisms of cinnamaldehyde and its congeners present in the cinnamon plant, Physiol. 3 (2) (2023) 173–207, https://doi.org/10.3390/physiologia3020013.

[32] S.H. Hong, I.A. Ismail, S.M. Kang, D.C. Han, B.M. Kwon, Cinnamaldehydes in cancer chemotherapy, Phytother Res. 30 (2016) 754–767, https://doi.org/10.1002/ptr.5592.

[33] F. Tian, C.T. Yu, W.D. Ye, Q. Wang, Cinnamaldehyde induces cell apoptosis mediated by a novel circular RNA hsa_circ_0043256 in non-small cell lung cancer, Biochem. Biophys. Res. Commun. 493 (3) (2017) 1260–1266, https://doi.org/10.1016/j.bbrc.2017.09.136.

[34] J. Park, S.H. Baek, Combination therapy with cinnamaldehyde and hyperthermia induces apoptosis of A549 non-small cell lung carcinoma cells via regulation of reactive oxygen species and mitogen-activated protein kinase family, Int. J. Mol. Sci. 21 (17) (2020) 1–15, https://doi.org/10.3390/ijms21176229.

[35] P.C. Anatole, *In vivo* anticancer activity of vanillin, benzophenone and acetophenone thiosemicarbazones on Swiss albino mice, J. Coast. Life Med. 2 (10) (2014) 811–816.

[36] M. Sadaqat, M. Qasim, M.T. ul Qamar, M.S. Masoud, U.A. Ashfaq, F. Noor, K. Fatima, K.S. Allemailem, F. Alrumaihi, A. Almatroudi, Advanced network pharmacology study reveals the multi-pathway and multi-gene regulatory molecular mechanism of *Bacopa monnieri* in liver cancer based on data mining, molecular docking, and microarray data analysis, Comput. Biol. Med. 161 (2023), https://doi.org/10.1016/j.compbiomed.2023.107059.

[37] Y.F. Wang, Y. Zheng, Y.Y. Cha, Y. Feng, S.X. Dai, S. Zhao, H. Chen, M. Xu, Essential oil of lemon myrtle (*Backhousia citriodora*) induces S-phase cell cycle arrest and apoptosis in HepG2 cells, J. Ethnopharmacol. 312 (2023) 116493, https://doi.org/10.1016/j.jep.2023.116493.

[38] S.A. Ahrendt, Y. Hu, M. Buta, M.P. McDermott, N. Benoit, S.C. Yang, L. Wu, D. Sidransky, p53 mutations and survival in stage I non-small-cell lung cancer: results of a prospective study, J. Natl. Cancer Inst. 95 (13) (2003) 961–970, https://doi.org/10.1093/jnci/95.13.961.

[39] B. Liu, Q. Liu, Y. Song, X. Li, Y. Wang, S. Wan, Z. Zhang, H. Su, Polymorphisms of HIF1A gene are associated with prognosis of early stage non-small-cell lung cancer patients after surgery, Med. Oncol. 31 (877) (2014) 1–9, https://doi.org/10.1007/s12032-014-0877-8.

[40] A. Taherkhani, P. Khodadadi, L. Samie, Z. Azadian, Z. Bayat, Flavonoids as strong inhibitors of MAPK3: a computational drug discovery approach, Int. J. Anal Chem. 2023 (2023) 1–16, https://doi.org/10.1155/2023/8899240.

[41] W. Liu, H. Wang, F. Bai, L. Ding, Y. Huang, C. Lu, S. Chen, C. Li, X. Yue, X. Liang, C. Ma, IL-6 promotes metastasis of non-small-cell lung cancer by up-regulating TIM-4 via NF-κB, Cell Prolif. 53 (3) (2020) 1–12, https://doi.org/10.1111/cpr.12776.

[42] E.M. Silva, V.S. Mariano, P.R.A. Pastrez, M.C. Pinto, A.G. Castro, K.J. Syrjanen, A. Longatto-Filho, High systemic IL-6 is associated with worse prognosis in patients with non-small cell lung cancer, PLoS One 12 (2017) 1–12, https://doi.org/10.1371/journal.pone.0181125.

[43] M. Olsson, B. Zhivotovsky, Caspases and cancer, Cell Death Differ. 18 (2011) 1441–1449, https://doi.org/10.1038/cdd.2011.30.

[44] R. Pradhan, G. Singhvi, S.K. Dubey, G. Gupta, K. Dua, MAPK pathway: a potential target for the treatment of non-small-cell lung carcinoma, Future Med. Chem. 11 (8) (2019) 793–795, https://doi.org/10.4155/fmc-2018-0468.

[45] A.S. Jain, A. Prasad, S. Pradeep, C. Dharmashekar, R.R. Achar, E. Silina, V. Stupin, R.G. Amachawadi, S.K. Prasad, R. Pruthvish, A. Syed, C. Shivamallu, S.P. Kollur, Everything old is new again: drug repurposing approach for non-small cell lung cancer targeting MAPK signaling pathway, Front. Oncol. 11 (2021) 1–15, https://doi.org/10.3389/fonc.2021.741326.

[46] Z. Lu, L. Ding, H. Hong, J. Hoggard, Q. Lu, Y.H. Chen, Claudin-7 inhibits human lung cancer cell migration and invasion through ERK/MAPK signaling pathway, Exp. Cell Res. 317 (13) (2011) 1935–1946, https://doi.org/10.1016/j.yexcr.2011.05.019.

[47] Y.J. Guo, W.W. Pan, S.B. Liu, Z.F. Shen, Y. Xu, L.L. Hu, ERK/MAPK signalling pathway and tumorigenesis, Exp. Ther. Med. 19 (2020) 1997–2007, https://doi.org/10.3892/etm.2020.8454.

[48] K. Kiełbowski, K. Ptaszyński, J. Wójcik, M.E. Wojtyś, The role of selected non-coding RNAs in the biology of non-small cell lung cancer, Adv. Med. Sci. 68 (1) (2023) 121–137, https://doi.org/10.1016/j.advms.2023.02.004.

[49] M.M. Suhail, W. Wu, A. Cao, F.G. Mondalek, K.M. Fung, P.T. Shih, Y.T. Fang, C. Woolley, G. Young, H.K. Lin, *Boswellia sacra* essential oil induces tumor cell-specific apoptosis and suppresses tumor aggressiveness in cultured human breast cancer cells, BMC complement. Altern. Med. 11 (129) (2011) 1–14. http://www.biomedcentral.com/1472-6882/11/129.

[50] X. Wang, Y. Lin, Tumor necrosis factor and cancer, buddies or foes? 1, Acta Pharmacol. Sin. 29 (11) (2008) 1275–1288, https://doi.org/10.1111/j.1745-7254.2008.00889.x.

[51] M.M. Pore, T.J.N. Hiltermann, F.A. Kruyt, Targeting apoptosis pathways in lung cancer, Cancer Lett. 332 (2) (2013) 359–368, https://doi.org/10.1016/j.canlet.2010.09.012.

[52] W. Sterlacci, M. Fiegl, A. Tzankov, Prognostic and predictive value of cell cycle deregulation in non-small-cell lung cancer, Pathobiology 79 (4) (2012) 175–194, https://doi.org/10.1159/000336462.

[53] J.W. Ma, T.C.Y. Tsao, Y.T. Hsi, Y.C. Lin, Y. Chen, Y. Chen, C.T. Ho, J.Y. Kao, T.D. Way, Essential oil of *Curcuma aromatica* induces apoptosis in human non-small-cell lung carcinoma cells, J. Funct.Foods 22 (2016) 101–112, https://doi.org/10.1016/j.jff.2016.01.019.

[54] C.C. Chen, Y. Chen, Y.T. Hsi, C.S. Chang, L.F. Huang, C.T. Ho, T.D. Way, J.Y. Kao, Chemical constituents and anticancer activity of *Curcuma zedoaria* roscoe essential oil against non-small cell lung carcinoma cells *in vitro* and *in vivo*, J. Agric. Food Chem. 61 (47) (2013) 11418–11427, https://doi.org/10.1021/jf4026184.

[55] D.T. Trang, T.K.V. Hoang, T.T.M. Nguyen, P. Van Cuong, N.H. Dang, H.D. Dang, T. Nguyen Quang, N.T. Dat, Essential oils of lemongrass (*Cymbopogon citratus* Stapf) induces apoptosis and cell cycle arrest in A549 lung cancer cells, BioMed Res. Int. 2020 (2020) 1–9, https://doi.org/10.1155/2020/5924856.

[56] A. Proboningrat, V.D. Kharisma, A.N.M. Ansori, R. Rahmawati, A. Fadholly, G.A.V. Posa, S.A. Sudjarwo, F.A. Rantam, A.B. Achmad, In silico Study of Natural inhibitors for Human papillomavirus-18 E6 protein, Res. J. Pharm. Technol. 15 (3) (2022) 1251–1256, https://doi.org/10.52711/0974-360X.2022.00209.

[57] L. Liu, Y. Jiao, M. Yang, L. Wu, G. Long, W. Hu, Network pharmacology, molecular docking and molecular dynamics to explore the potential immunomodulatory mechanisms of deer antler, Int. J. Mol. Sci. 24 (12) (2023) 10370, https://doi.org/10.3390/ijms241210370.

[58] A. Taherkhani, P. Khodadadi, L. Samie, Z. Azadian, Z. Bayat, Flavonoids as strong inhibitors of MAPK3: a computational drug discovery approach, Int. J. Anal. Chem. (2023) 2023, https://doi.org/10.1155/2023/8899240.

[59] M.H. Widyananda, S.K. Pratama, A.N.M. Ansori, Y. Antonius, V.D. Kharisma, A.A.A. Murtadlo, V. Jakhmola, M. Rebezov, M. Khayrullin, M. Derkho, E. Ullah, Quercetin as an anticancer candidate for glioblastoma multiforme by targeting AKT1, MMP9, ABCB1, and VEGFA: an *in silico* study, Karbala Int. J. Mod. Sci. 9 (3) (2023) 1–12, https://doi.org/10.33640/2405-609X.3312.

[60] T. Maradesha, R.M. Martiz, S.M. Patil, A. Prasad, A.T. Babakr, E. Silina, V. Stupin, R.R. Achar, R. Ramu, Integrated network pharmacology and molecular modeling approach for the discovery of novel potential MAPK3 inhibitors from whole green jackfruit flour targeting obesity-linked diabetes mellitus, PLoS One 18 (1) (2023) 1–24, https://doi.org/10.1371/journal.pone.0280847.

[61] A.F. Dibha, S. Wahyuningsih, A.N.M. Ansori, V.D. Kharisma, M.H. Widyananda, A.A. Parikesit, M.T. Sibero, R.T. Probojati, A.A.A. Murtadlo, J.P. Trinugroho, T. H. Sucipto, Utilization of secondary metabolites in algae Kappaphycus alvarezii as a breast cancer drug with a computational method, Phcog. J. 14 (3) (2022), https://doi.org/10.5530/pj.2022.14.68.

[62] H. Lafridi, F.A. Almalki, T. Ben Hadda, M. Berredjem, S.M. Kawsar, A.M. Alqahtani, E.R. Esharkawy, B. Lakhrissi, H. Zgou, *In silico* evaluation of molecular interactions between macrocyclic inhibitors with the HCV NS3 protease. Docking and identification of antiviral pharmacophore site, J. Biomol. Struct. Dyn. 41 (6) (2023) 2260–2273, https://doi.org/10.1080/07391102.2022.2029571.

[63] S. Grine, F. Taibi, M. Berredjem, A. Dekir, F. Benaliouche, K.O. Rachedi, A. Acidi, N. Iqbal, V. Niranjan, C. Lavanya, N. Soltani, Antifungal activity of the essential oil of *Pelargonium graveolens*. Molecular docking, molecular dynamics, DFT, and *in silico* ADMET studies of five derivatives, J. Mol. Struct. (2) (2023) 1294, https://doi.org/10.1016/j.molstruc.2023.136546.

[64] P. Politzer, J.S. Murray, The fundamental nature and role of the electrostatic potential in atoms and molecules, Theor. Chem. Acc. 108 (2002) 134–142, https://doi.org/10.1007/s00214-002-0363-9.

[65] N. Islam, D.C. Ghosh, On the electrophilic character of molecules through its relation with electronegativity and chemical hardness, Int. J. Mol. Sci. 13 (2012) 2160–2175, https://doi.org/10.3390/ijms13022160.

[66] Y. Zu, H. Yu, L. Liang, Y. Fu, T. Efferth, X. Liu, N. Wu, Activities of ten essential oils towards *Propionibacterium acnes* and PC-3, A-549 and MCF-7 cancer cells, Molecules 15 (5) (2010) 3200–3210, https://doi.org/10.3390/molecules15053200.

[67] A. Alam, M.J. Ansari, M.H. Alqarni, M.A. Salkini, M. Raish, Antioxidant, antibacterial, and anticancer activity of ultrasonic nanoemulsion of *Cinnamomum Cassia* L, Essential Oil. Plants. 12 (4) (2023) 1–15, https://doi.org/10.3390/plants12040834.

[68] B. Justus, C.C. Kanunfre, J.M. Budel, M.F. de Faria, V. Raman, J.P. de Paula, P.V. Farago, New insights into the mechanisms of French lavender essential oil on non-small-cell lung cancer cell growth, Ind. Crops Prod. 136 (2019) 28–36, https://doi.org/10.1016/j.indcrop.2019.04.051.

[69] P. Hansakul, K. Aree, S. Tanuchit, A. Itharat, Growth arrest and apoptosis via caspase activation of dioscoreanone in human non-small-cell lung cancer A549 cells, BMC Compl. Alternative Med. 14 (413) (2014) 1–12, https://doi.org/10.1186/1472-6882-14-413.

[70] J. Li, H.Y. Huang, Y.C.D. Lin, H. Zuo, Y. Tang, H.D. Huang, *Cinnamomi ramulus* inhibits cancer cells growth by inducing G2/M arrest, Front. Pharmacol. 14 (2023) 1–15, https://doi.org/10.3389/fphar.2023.1121799.

[71] Y. Shi, A structural view of mitochondria-mediated apoptosis, Nat. Struct. Biol. 8 (5) (2001) 394–401, https://doi.org/10.1038/87548.

[72] R. Vanajothi, A. Sudha, R. Manikandan, P. Rameshthangam, P. Srinivasan, *Luffa acutangula* and *Lippia nodiflora* leaf extract induces growth inhibitory effect through induction of apoptosis on human lung cancer cell line, Biomed. Prev. Nutr. 2 (4) (2012) 287–293, https://doi.org/10.1016/j.bionut.2012.03.002.

[73] B.F. Chu, H.C. Lin, X.W. Huang, H.Y. Huang, C.P. Wu, M.C. Kao, An ethanol extract of *Poria cocos* inhibits the proliferation of non-small cell lung cancer A549 cells via the mitochondria-mediated caspase activation pathway, J. Funct.Foods 23 (2016) 614–627, https://doi.org/10.1016/j.jff.2016.03.016.

[74] Y. Song, Y. Miao, C.P. Song, Behind the scenes: the roles of reactive oxygen species in guard cells, New Phytol. 201 (4) (2014) 1121–1140, https://doi.org/10.1111/nph.12565.

[75] C.C. Zhang, C.G. Li, Y.F. Wang, L.H. Xu, X.H. He, Q.Z. Zeng, C.Y. Zeng, F.Y. Mai, B. Hu, D.Y. Ouyang, Chemotherapeutic paclitaxel and cisplatin differentially induce pyroptosis in A549 lung cancer cells via caspase-3/GSDME activation, Apoptosis 24 (2019) 312–325, https://doi.org/10.1007/s10495-019-01515-1.

[76] P.C. Rao, S. Begum, M. Sahai, D.S. Sriram, Coptisine-induced cell cycle arrest at G2/M phase and reactive oxygen species–dependent mitochondria-mediated apoptosis in non-small-cell lung cancer A549 cells, Tumor Biol. 39 (2017) 1–13, https://doi.org/10.1177/1010428317694565.

[77] D.R. McIlwain, T. Berger, T.W. Mak, Caspase functions in cell death and disease, Cold Spring Harbor Perspect. Biol. 5 (2013) 1–30, https://doi.org/10.1101/cshperspect.a008656.